scientific reports

Check for updates

OPEN

Multiple omics integrative analysis identifies *GARS1* as a novel prognostic and immunological biomarker: from pan-cancer to bladder cancer

Weihui Liu[1,2,6], Chengcheng Wei[3,4,6], Qingliu He[2], Zhaohui Chen[3], Wei Zhuang[2], Yihong Guo[2]✉ & Xueyi Xue[5]✉

Glycyl-tRNA synthetase (*GARS1*) is differentially expressed across cancers. In this study, the value of GARS1 in the diagnosis and prognosis of various cancers was comprehensively evaluated by multiple omics integrative pan-cancer analysis and experimental verification. Through Kaplan–Meier, ROC and multiple databases, we explored *GARS1* expression and prognostic and diagnostic patterns across cancers. The *GARS1* relative reaction network was identified in PPI, GO, KEGG, methylation models and the genetic mutation atlas. Further research on the *GARS1* value in bladder urothelial carcinoma (BLCA) was conducted by regression and nomogram models. We further analyzed the correlation between *GARS1* and immune markers and cells in BLCA. Finally, in vitro experiments were used to validate *GARS1* the oncogenic function of *GARS1* in BLCA. We found that *GARS1* was highly expressed across cancers, especially in BLCA. *GARS1* expression was correlated with poor survival and had high diagnostic value in most tumor types. *GARS1* is significantly associated with tRNA-related pathways whose mutation sites are mainly located on tRNA synthetase. In addition, Upregulation of *GARS1* was connected with immune cell infiltration and five key MMR genes. M2 macrophages, TAMs, Th1 and T-cell exhaustion, and marker sets associated with *GARS1* expression indicated specific immune infiltration in BLCA. Finally, in vitro experiments validated that *GARS1* expression promotes BLCA cell proliferation and metastasis and inhibits apoptosis. Overall, *GARS1* can be a novel prognostic and immunological biomarker through multiple omics integrative pan-cancer analysis. The expression of *GARS1* in BLCA was positively correlated with specific immune infiltration, indicating that *GARS1* might be related to the tumor immune microenvironment.

Keywords *GARS1*, Pan-cancer, Bladder cancer, Multiple omics, Immune infiltration

Cancer remains the leading cause of death worldwide, highlighting the urgent need for prognostic biomarkers to guide treatment decisions[1]. Platinum-based chemotherapy is the standard regimen for bladder cancer; however, approximately 50% of patients are not suitable candidates due to various issues, including renal insufficiency, complications, age, and poor physical condition[2]. Immune checkpoint inhibitors (ICIs) have been approved as a first-line treatment for PD-L1-positive metastatic bladder urothelial cancer (mBLCA) in patients who cannot tolerate cisplatin, as well as for use as a second-line therapy following progression after cisplatin treatment[3]. Despite bladder cancer being a highly immunogenic tumor, only a subset of mBLCA patients benefit from ICI therapy. The underlying mechanisms for this variability in response to ICI treatment remain poorly understood[4]. Additionally, immune-related adverse events, such as liver function impairment, can adversely affect treatment

[1]Department of Urology, The First Affiliated Hospital of Fujian Medical University, Fuzhou 350005, China. [2]Department of Urology, The Second Affiliated Hospital of Fujian Medical University, Quanzhou 362000, China. [3]Department of Urology, Union Hospital, Tongji Medical College, Huazhong University of Science and Technology, Wuhan 430074, China. [4]Department of Urology, The First Affiliated Hospital of Chongqing Medical University, Chongqing 404100, China. [5]Department of Urology, Urology Research Institute, The First Affiliated Hospital of Fujian Medical University, Fuzhou 350005, China. [6]These authors contributed equally: Weihui Liu and Chengcheng Wei. ✉email: hotniu@fmu.edu.cn; cmd15205014314@163.com

outcomes[5,6]. Currently, many clinicians rely on biomarkers of immunotherapy response, such as PD-L1 expression in specific malignant tumors, to predict treatment efficacy[7]. However, due to the heterogeneity of PD-L1 expression and the lack of standardized detection methods, the predictive value of PD-L1 positivity in mBLCA patients is considered unreliable[8]. Recent research suggests that serum albumin levels may serve as a prognostic biomarker for patients with advanced cancer undergoing ICI treatment[9]. In 2019, the Bladder Cancer Molecular Taxonomy Group[10] classified bladder cancer into six subtypes: luminal papillary (24%), luminal nonspecified (8%), luminal unstable (15%), stroma-rich (15%), basal/squamous (35%), and neuroendocrine-like (3%). This classification requires further clinical validation. Therefore, there is an urgent need to identify significant and effective biomarkers to predict immune efficacy in mBLCA patients.

Aminoacyl-tRNA synthetases (ARSs) are an ancient family of 20 important enzymes. In the process of protein synthesis, ARSs link tRNAs to corresponding amino acids[11,12]. ARSs play essential roles in various cells, and catalyze the tRNA substrate aminoacylation in a two-step reaction. The first step is to juxtapose ATP, amino acids, and tRNAs. Then, ARSs produce aminoacylate tRNAs for protein synthesis through the ribosome[13–15]. Glycyl-tRNA synthetase (*GARS1*) belongs to the class II type, which is characterized by three conserved signature motifs, and unlike other ARSs, the quaternary structure of *GARS1* is not phylogenetically conserved[16,17]. In recent years, increasing evidence has indicated that the multiple functions of Ars are controlled by complex mechanisms to respond to different cellular stimuli as translational components and important factors in controlling rapidly emerging tumorigenesis[18,19]. *GARS1*, as an ancient enzyme, may provide new insights into the cancer process and has become a potential therapeutic target[20]. However, the possible roles and function of *GARS1* in tumor types have not been reported before.

The tumor microenvironment (TME) has different types of cells, including immune cells, stromal cells, cancer-associated fibroblasts and endothelial cells. To some extent, the TME influences the therapeutic response and clinical outcome[21,22]. Current studies have illustrated the important roles and prognostic value of infiltrating immune cells in malignant tumor progression[23,24]. Immunotherapy has been developed as an increasing alternative anticancer treatment strategy to stimulate and adapt the innate immune systems for a strong antitumoral immune response[25,26]. For instance, in the clinic, cytotoxic T lymphocyte-associated antigen 4 (CTLA4) and programmed death-1 (PD-1) are usually employed as small-molecule anticancer inhibitors[27,28]. Unfortunately, immunotherapies now only respond well to certain types of cancer and are limited to some patients[29]. Thus, it is necessary to explore potential targets for further treatment. The relationship between *GARS1* expression and the infiltrating immune situation has not been explored.

In this study, we performed multiple omics integrative analyses of *GARS1* across cancers using The Cancer Genome Atlas (TCGA) and GTEx databases. Potential relationships between *GARS1* expression and immune infiltration levels and immune co-expression analysis were investigated. Furthermore, we tested and verified *GARS1* as a novel prognostic and immunological biomarker in bladder cancer and.

Methods and materials

GARS1 Expression Level

The Cancer Genome Atlas (TCGA) (https://portal.gdc.cancer.gov/) provides pan-cancer RNA sequencing information from 11,069 samples for free[30]. GTEx (https://commonfund.nih.gov/) provides 31 types of normal tissue gene expression data[31]. The cell line expression level matrix of *GARS1* was obtained from the CCLE database (https://portals.broadinstitute.org/ccle/) which provided models for studying cancer biology and validating cancer targets[32]. Gene Expression Profiling Interactive Analysis 2 (GEPIA2) (http://gepia2.cancer-pku.cn) was designed as an online tool to analyze RNA sequencing, including 60,498 genes and 198,619 isoforms[33]. We used GEPIA2 to evaluate *GARS1* expression 33 types of tumor tissues matched with 31 standard normal tissues based on TCGA and GTEx. Data about *GARS1* expression levels in 21 tumor cell lines were obtained from the Cancer Cell Line Encyclopedia (CCLE) (https://www.broadinstitute.org/ccle)[34].

Immunohistochemistry (IHC) and protein expression of GARS1

The Human Protein Atlas (HPA) (https://www.proteinatlas.org/) is designed as a database using integrated omics technologies to offer proteomic and transcriptome information, including cell, tissue and pathology Atlas[35]. Protein immunohistochemistry (IHC) images were downloaded from HPA to evaluate *GARS1* protein expression on specific tumors and normal tissues. Then, we used a web tool of UALCAN (http://ualcan.path.uab.edu/analysis-prot.html) to access various cancer protein expressions consisting of Colon, Breast cancer, Ovarian Renal and Uterine corpus endometrial from Clinical Proteomic Tumor Analysis Consortium (CPTAC) Confirmatory/Discovery database[36].

Prognosis, diagnosis and relative clinical phenotype analysis

We obtained information including survival data and relative clinical phenotypes from the TCGA database, which was downloaded from the UCSC Xena (https://xenabrowser.net/datapages/) database[37]. We used three indicators, OS, DSS and PFI, to access the prognostic ability of *GARS1*. The K-M was employed for survival analyses, and ROC curves were employed for diagnostic performance using the pROC package.

Regression analysis in BLCA estimated the risk of death using Cox modeling and $p < 0.05$ was considered statistically significant. Based on clinical phenotype, we constructed a nomogram for predicting BLCA OS and validated the results by the Calibration model.

Protein–protein interaction network

We used the Search Tool for the Retrieval of Interacting Genes/Proteins (STRING) website (https://string-db.org/) as another online tool to predict potential protein–protein interactions. STRING contains a large host

of protein–protein integrated and consolidated data, including direct (physical) and indirect (functional) correlations. We imported *GARS1* into STRING to construct a PPI network with no more than 10 interactors. We selected confidence scores > 0.9, which means highly significant.

Genetic feature analysis

cBioportal for Cancer Genomics (http://www.cbioportal.org) was used to evaluate the genetic features of *GARS1* including deep deletion, somatic mutations and amplification[38]. We first queried *GARS1* into "TCGA Pan-Cancer Atlas Studies" to assess *GARS1* genetic alteration frequencies and visualized the results via the "Cancer Types Summary" module. Then, we used the "Mutations" module to determine the mutation type and mutation site of *GARS1*. We also drew the mutation spectrum of *GARS1* across the TCGA pan-caner dataset via the "OncoPrint" module. R software and package tidyverse were used to conduct the co-expression analysis between *GARS1* and five key MMR genes.

DNA methylation analysis

DNA methylation influences gene expression and function, which impacts the clinical outcome, prognosis and carcinogenesis. MethSurv (https://biit.cs.ut.ee/methsurv/) is a web portal that analyses DNA methylation biomarkers[39]. DNA methylation of *GARS1* at CpG sites in BLCA was analyzed by MethSurv. The promoter methylation level of GARS between various types of BLCA samples was analyzed by the UALCAN database.

Gene pathway analysis

Gene Ontology (GO) functional analysis aims to annotate genes to identify characteristic biological attributes based on high-flux transcriptome and gene data[40]. The Kyoto Encyclopedia of Genes and Genomes (KEGG) is a substant database that includes genes, biological pathways, drugs and disease information[41–44]. GO and KEGG analyses were conducted for 50 *GARS1*-binding proteins, visualized by the ggplot2 package for visualization and statistically analyzed by the cluster-Profiler package. GSEA was used as a computational method to determine whether gene expression was statistically significant and concordant between various biological states[45]. The package Cluster Profiler was used to identify excessive functions and pathway varieties between different *GARS1* expression levels in BLCA. Each analysis was repeated 5000 times. FDR < 0.05 and higher NES results were considered potential pathways that were chosen.

Immune infiltration analysis

Pan-cancer analysis of the correlation between *GARS1* expression and infiltrating immune cells was conducted by ssGSEA with the R package GSVA (version 3.6)[46]. Twenty-four types of immune cell infiltration levels were quantified from 33 types of cancers. Spearman and Wilcoxon rank-sum tests were used to identify relationships between pan-cancers and immune cell subsets. Then, Pearman correlation analysis was performed to assess the co-expression of *GARS1* with immune genes including immune-associated genes, MHC genes, chemokines, chemokine receptors, immune activation genes and immunosuppressive genes in 33 cancer types. The results were displayed as heatmaps using the R package "pheatmap". GEPIA2 contains 9736 tumor and 8587 normal sample RNA sequencing expression data and 60,498 gene and 198,619 isoform information. The Tumor Immune Estimation Resource (TIMER2) is a systemic database that includes 10,897 samples for immune infiltrate analysis (http://cistrome.org/TIMER/)[47]. We used GEPIA2 to investigate *GARS1* expression in connection with immune cell markers and then we identified the gene with a significant correlation with *GARS1* through TIMER2.

Reverse transcription-quantitative PCR

TRIzol reagent was used to extract RNA (Invitrogen, Carlsbad, CA, USA) and reverse transcribed into cDNA using the iScript cDNA synthesis kit (Bio-Rad, Hercules, CA, USA). qRT-PCR was performed with ChamQ SYBR qPCR Master Mix (Vazyme, Nanjing, China) with a StepOne Plus real-time PCR system (Life Technologies, CA, USA). After standardization of the GAPDH gene, the gene expression was calculated according to the $2^{-\Delta\Delta Ct}$ method. The sequences of primer used in the present study are listed in Supplementary Table S1.

Cell culture and transfection

We purchased cell lines, including RT4, T24, and T24T from ATCC, EJ-1 from JCRB which were confirmed by STR profiling. Cell lines were incubated in DMEM with 10% 1% penicillin–streptomycin plus FBS (Hyclone, USA). Jima Biotech (Suzhou, China) constricted *GARS1* overexpression plasmids and shRNA against *GARS1*. The cell lines were transfected with Lipofectamine 2000 reagent (Invitrogen, USA) according to the manufacturer's protocols.

Migration, proliferation, invasion, and apoptosis assays

CCK-8 and colony formation assays were used to monitor cell proliferation in vitro. EJ, RT4, T24, and T24T cell lines were seeded in 96-well plates (2500 cells/well) for 24 h. We recorded the optical density (OD) absorption value at 450 nm daily. Then, we seeded the cell line in a 6-well plate at 1000 cells/well for colony formation and changed the medium every 4 days.

We used 24-well Transwell chambers (Corning Life Sciences) to evaluate cell invasion and migration ability. We added 500 µl complete medium in the lower chambers and 200 µl serum-free medium with 4×10^4 cells in the upper chamber. In the invasion assay, chamber inserts were precoated with 50 µl Matrigel matrix (BD Biosciences, Sparks, MD). After incubation for 24 h or the migration assay and 48 h of invasion assay at 37 °C, we removed cells remaining in the upper chamber. The invasive and migratory cells were fixed and stained with

0.1% crystal violet at the lower surface of the chamber. Invasive or migratory cells were counted under an inverted phase-contrast microscope (Olympus, Tokyo, Japan) at 200× magnification.

In the apoptosis assay, we seeded cells in 6-well plates at 90% confluency. Then, we resuspended the collected cells in binding buffer at a concentration of 1×10^6 cells/mL. We mixed 5 mL Annexin V-PE and 5 mL 7-AAD for 15 min. The results of apoptotic cells were analyzed by FACSVerse (Becton, Dickinson, and Company) in BD FACSuite software.

Western blot

We extracted total protein of seven cell lines and SV cell using RIPA lysis buffer. Subsequently, the proteins were incubated overnight at 4 °C on a PVDF membrane with the following primary antibodies: anti-β-Actin (1:1000, Abcam, USA) and anti-GARS1 (1:1000, Abcam, USA).

Statistical analysis

We normalized gene expression data by log2 transformation. *t*-tests were used to evaluate comparisons between normal and cancer tissues. Kaplan–Meier analysis, and Cox, and log-rank tests were used to conduct survival analysis. Spearman's test or Pearson's test was used to conduct correlation analysis; $p < 0.05$ was defined as significant difference. R software was used to conduct all statistical analyses (Version 4.0.2).

Results

GARS1 expression levels across various cancers

The *GARS1* expression levels were assessed between pan-cancer and normal tissues from the TCGA and GTEx datasets using GEPIA2 database (Fig. 1a). The expression level was higher in 12 tumors compared with the normal tissues, including Bladder Urothelial Carcinoma (BLCA), Colon-Adenocarcinoma (COAD), Lymphoid neoplasm diffuse B-cell lymphoma (DLBC), Esophageal carcinoma (ESCA), Liver Hepatocellular Carcinoma (LIHC), Pancreatic adenocarcinoma (PAAD), Rectum adenocarcinoma (READ), Stomach adenocarcinoma (STAD), Testicular germ cell tumors (TGCT), Thymoma (THYM), Uterine Corpus Endometrial Carcinoma (UCEC), and Uterine carcinosarcoma (UCS) (Fig. 1b–m). Interestingly, the expression level of *GARS1* in Acute myeloid leukemia (LAML) was lower than that in normal tissue (Fig. 1n). Research based on CCLE database showed that GARS1mRNA is highly expressed in many cancer cell lines, which is consistent with tissue expression (Fig. 2m).

GARS1 protein expression levels between tumor and normal tissue samples

From the images in the HPA database, we found that normal bladder, liver and endometrioma tissues had weak or no *GARS1* IHC staining, while tumor tissues had strong staining. Normal colon, stomach and testicular tissues had moderate *GARS1* staining, which was located in mucous membrane, but COAD, STAD, TGCT had strong *GARS1* staining and hard to identify the normal structure (Fig. 2a–f). From the results of the CPTAC dataset, higher expression of *GARS1* total protein was observed in breast cancer, clear cell RCC, colon cancer, ovarian cancer, lung adenocarcinoma and UCEC than in normal tissues (Fig. 2g–l).

Pan-cancer prognostic value of GARS1

Overall survival (OS) Cox analysis showed that *GARS1* expression was correlated with OS in ACC ($p = 0.001$), BLCA ($p = 0.001$), BRCA ($p < 0.001$), Head and neck squamous cell carcinoma (HNSC) ($p = 0.012$), Kidney chromophobe (KICH) ($p = 0.026$), Kidney renal clear cell carcinoma (KIRP) ($p = 0.021$), lower grade glioma (LGG) ($p = 0.004$), LIHC ($p = 0.002$), Lung adenocarcinoma (LUAD) ($p = 0.007$), mesothelioma (MESO) ($p = 0.001$), Sarcoma (SARC) ($p = 0.004$), UCEC ($p = 0.004$), and THYM ($p = 0.029$) (Fig. 3). We found that *GARS1* expression was a high-risk indicator in ACC, BLCA, BRCA, HNSC, KICH, KIRP, LGG, LIHC, LUAD, MESO, PAAD, SARC, UCEC, especially in ACC (Fig. 3a, hazard ratio = 4.61) and KICH (Fig. 3a, hazard ratio = 10.57). Additionally, patients with high *GARS1* expression displayed decreased survival in ACC (Fig. 3b, $p = 0.001$), BLCA (Fig. 3c, $p = 0.001$), BRCA (Fig. 3d, $p < 0.001$), HNSC (Fig. 3e, $p = 0.012$), KICH (Fig. 3f, $p = 0.026$), KIRP (Fig. 3g, $p = 0.021$), LGG (Fig. 3h, $p = 0.004$), LIHC (Fig. 3i, $p = 0.002$), LUAD (Fig. 3j, $p = 0.007$), MESO (Fig. 3k, $p = 0.001$), SARC (Fig. 3l, $p = 0.004$), UCEC (Fig. 3m, $p = 0.004$) as analyzed by Kaplan–Meier analyses. Conversely, high *GARS1* expression levels were associated with increased survival in THYM (Fig. 3n, $p = 0.029$).

Moreover, we also constructed models of disease-specific survival (DSS) (Supplementary Fig. 1), which revealed a correlation between higher *GARS1* expression and poor prognosis in ACC, BLCA, BRCA, CESC, KIRP, LGG, LIHC, MESO, SARC, UCEC, and UVM. Furthermore, forest plots and KM survival analysis showed associations between the high expression of *GARS1* and poor PFI in various cancers including ACC, BLCA, BRCA, NHSC, KICH, KIRP, LGG, LIHC, LUAD, MESO, PRAD, SARC, and UVM (Supplementary Fig. 2).

Pan-cancer diagnostic value of GARS1

The receiver operating characteristic (ROC) curve was used to access discriminative power in identifying tumors from normal cells across cancers. The expression of *GARS1* had AUC values of 0.946, 0.923, 0.969, 0.944, 0.909, 0.980, 0.948, 0.985, 0.913, and 0.936 in BLCA, BRCA, COAD, ESCA, KIRP, READ, STAD, TGCT, UCEC, and UCS respectively, which indicated high accuracy. The expression of *GARS1* had AUC values of 0.834, 0.892, 0.846, 0.831, and 0.882 in ACC, CESC, GBM, KICH, and LIHC, respectively, which indicated a certain accuracy (Fig. 4).

Construction of the GARS1 protein–protein interaction network in pan-cancer

To further explore possible *GARS1*-related metabolism and molecular mechanisms, we constructed the *GARS1* protein–protein interaction network across cancers based on the STRING database (Fig. 5a). The PPI network

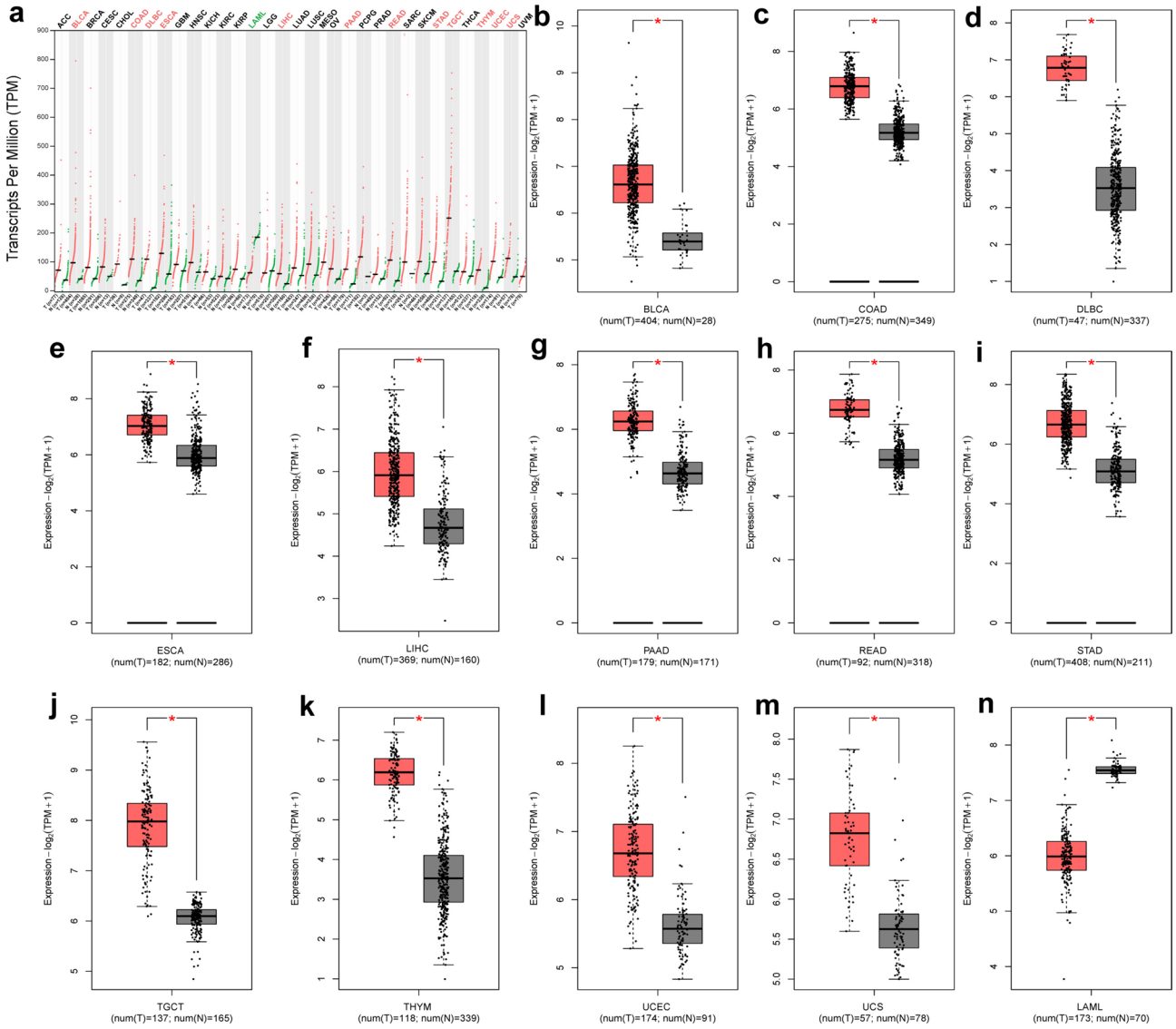

Figure 1. Pan-cancer expression analysis of *GARS1*. (**a**) *GARS1* expression level between tumor and normal tissues in pan-cancer data of TCGA and GTEx using GEPIA2. (**b**–**n**) The expression level of *GARS1* in Bca, COAD, DLBC, ESCA, LIHC, PAAD, READ, STAD, TGCT, THYM, UCEC, UCS and LAML. * was considered statistically significant.

showed the relationships and annotations of *GARS1*-related proteins. We listed the top 10 related gene corresponding gene names with their annotation scores (Fig. 5b). IARS, AARS, EPRS, GPHN, YARS, TARS, NARS, SARS, TARSL2, and KARS were the top 10 proteins related to *GARS1*. These proteins are almost all the aminoacyl-tRNA synthetases that participate in protein synthesis.

Gene ontology and Kyoto encyclopedia of genes and genomes enrichment analyses

We conducted Kyoto Encyclopedia of Genes and Genomes (KEGG) enrichment analysis and Gene Ontology (GO) analysis of *GARS1*-binding proteins to identify possible signaling pathways. The results were visualized by the ggplot2 package, and the cluster Profiler package was used for statistical analysis (Fig. 5c–e). Pathways of mitotic nuclear division and Aminoacyl-tRNA biosynthesis were the pathways most related to *GARS1*.

The genetic features of GARS1 in pan-cancers

Next, we have examined the genetic alterations of *GARS1* in cbioportal for Cancer Genomics (http://www.cbioportal.org), which includes TCGA pan-cancer datasets. The overall genetic alteration rate of *GARS1* is relatively low (1.6%) across cancers. Endometrial Carcinoma demonstrated the highest genetic alteration rate of *GARS1* (5.46%), followed by Bladder Urothelial Carcinoma (3.65%) (Fig. 6a). The mutation site of *GARS1* was mainly located on the tRNA synthetase class II core domain but no hot spot mutation site of *GARS1* was detected in pan-caner (Fig. 6b). Missense mutations were the main genetic alterations type of *GARS1* and most mutations were C>T (Fig. 6c). We observed copy number variations (CNVs) of *GARS1*, and amplification was frequently

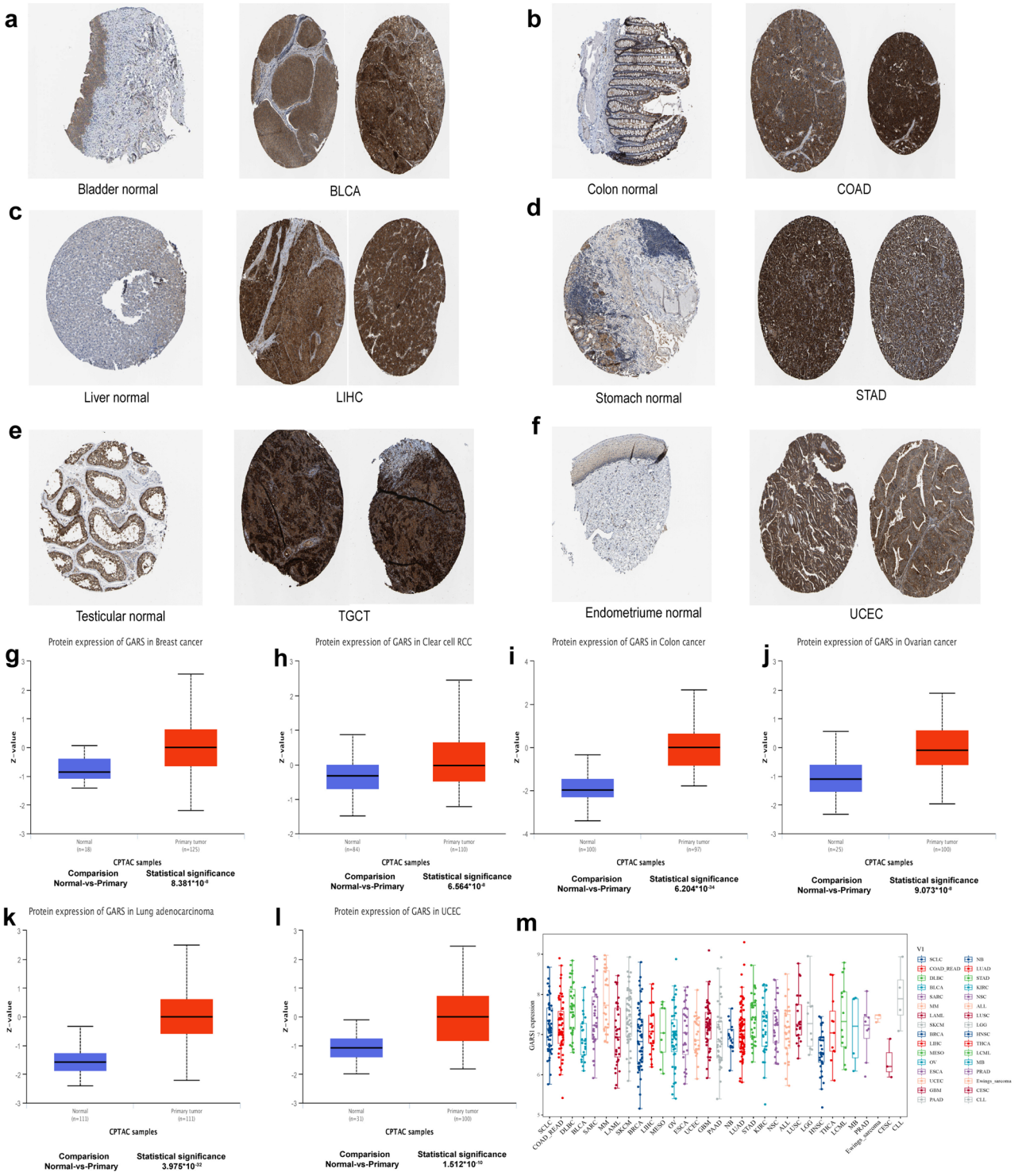

Figure 2. Immunohistochemistry images. *GARS1* expression was higher in (**a**) Bladder Urothelial Carcinoma (BLCA), (**b**) Colon-Adenocarcinoma (COAD), (**c**) Liver Hepatocellular Carcinoma (LIHC), (**d**) Stomach adenocarcinoma (STAD), (**e**) Testicular germ cell tumors (TGCT), (**f**) Uterine Corpus Endometrial Carcinoma (UCEC); Based on the CPTAC dataset, the expression level of *GARS1* total protein was analyzed between normal tissue and primary tissue of (**g**) Breast Cancer, (**h**) Clear Cell RCC, (**i**) Colon Cancer, (**j**) Ovarian Cancer, (**k**) Lung adenocarcinoma and (**l**) UCEC. $p < 0.001$ was considered statistically significant, (**m**) The expression level of *GARS1* in tumor cell lines.

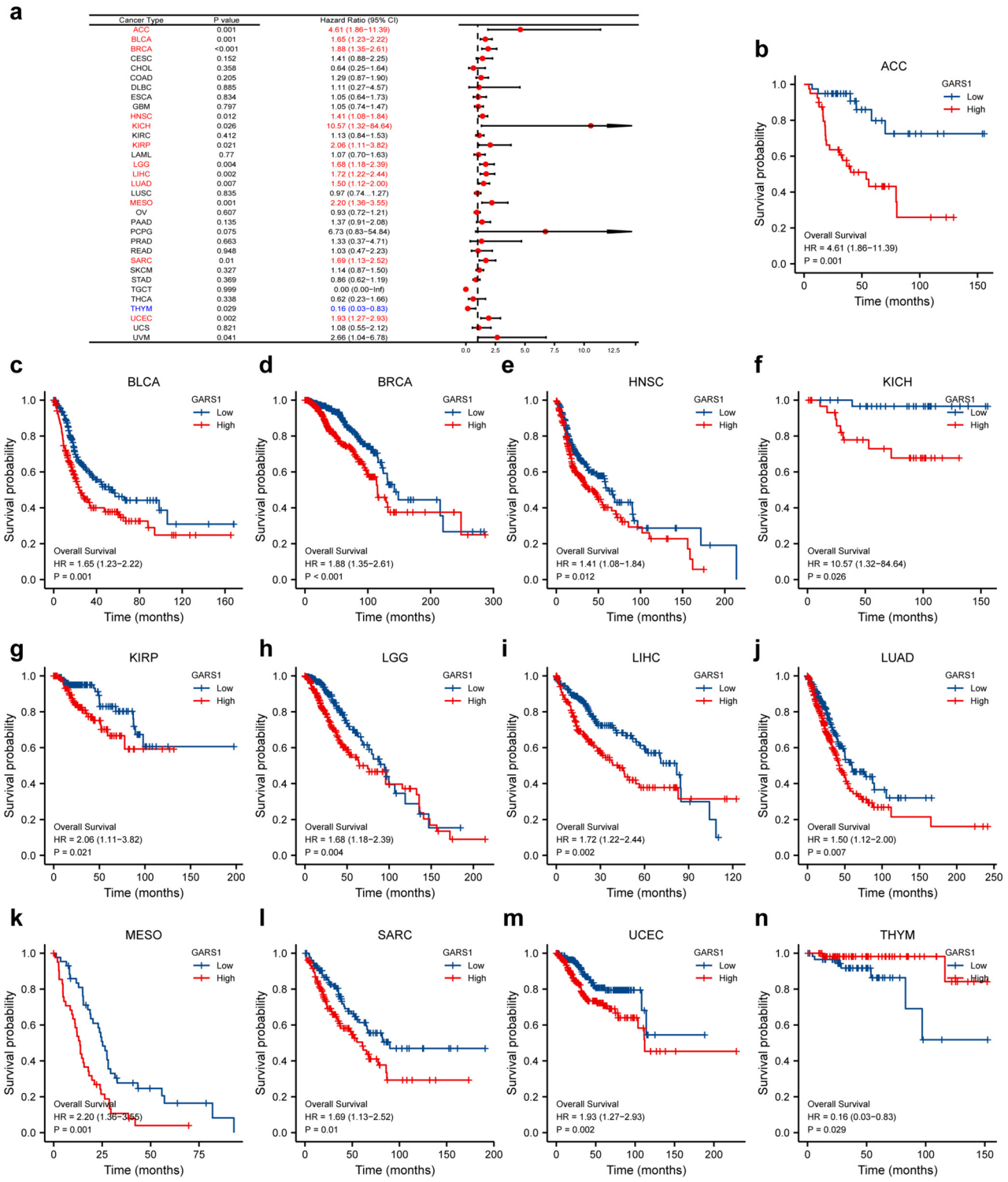

Figure 3. The expression of *GARS1* associated with OS. (**a**) Forest plots between OS and *GARS1* in pan-cancer. (**b**) Kaplan–Meier curves of ACC, (**c**) BLCA, (**d**) BRCA, (**e**) HNSC, (**f**) KICH, (**g**) KIRP, (**h**) LGG, (**i**) LIHC, (**j**) LUAD, (**k**) MESO, (**l**) SARC, (**m**) UCEC, (**n**) UVM, and (**o**) THY.

observed in colorectal adenocarcinoma (2.75%), esophagogastric adenocarcinoma (2.11%) and bladder urothelial carcinoma (1.95%) (Fig. 6c). Furthermore, correlation analysis indicated that the expression of *GARS1* was significantly and positively associated with the mutation levels of four of five key mismatch repair (MMR), MLH1, MSH2, MSH6 and PMS2, across the cancers (Fig. 6d).

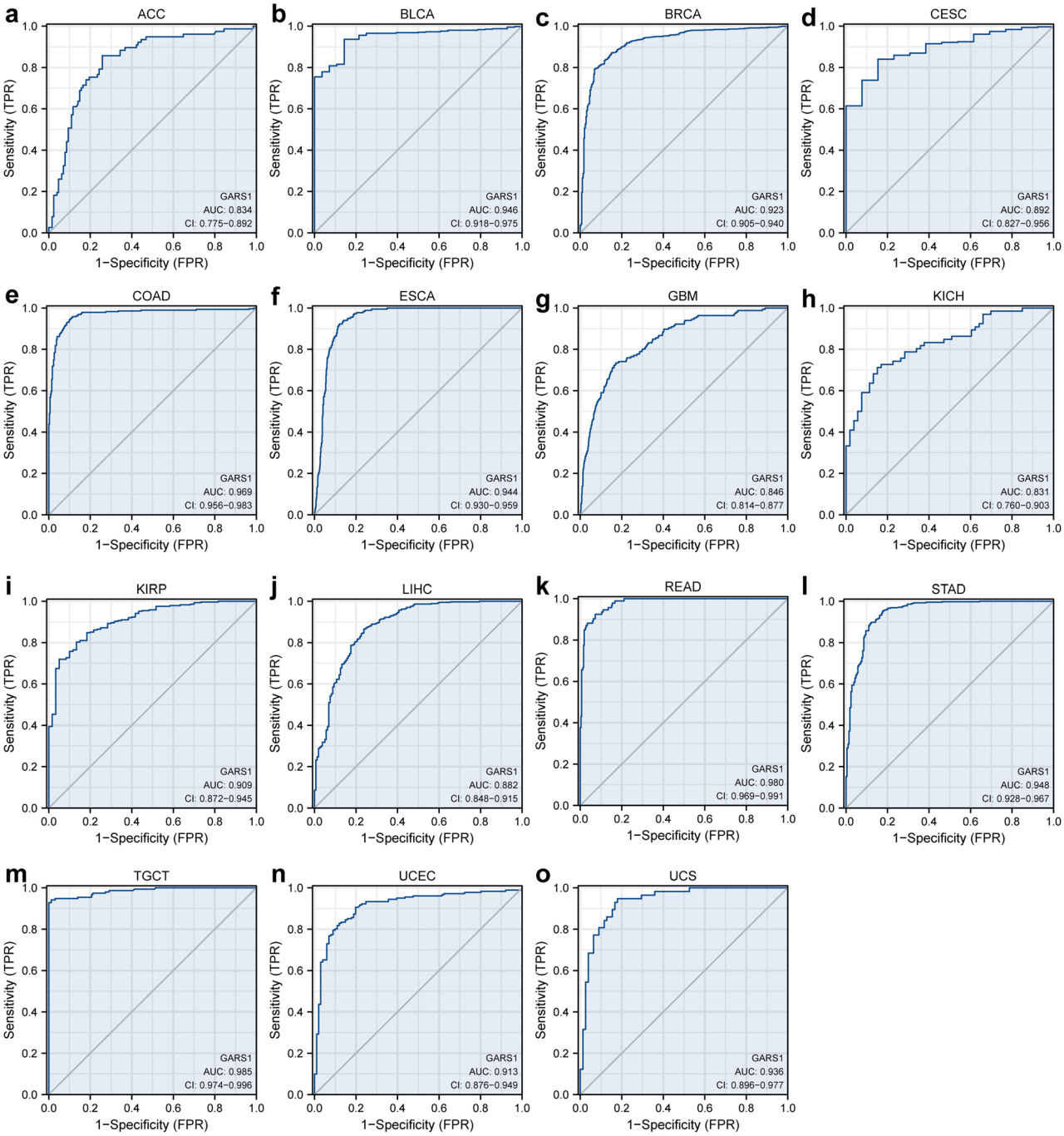

Figure 4. Correlation between *GARS1* expression and receiver operating characteristic (ROC) curve for *GARS1* expression in pan-cancer. (**a**) ACC, (**b**) BLCA, (**c**) BRCA, (**d**) CESC, (**e**) COAD, (**f**) ESCA, (**g**) GBM, (**h**) KICH, (**i**) KIRP, (**j**) LIHC, (**k**) READ, (**l**) STAD, (**m**) TGCT, (**n**) UCEC, (**o**) UCS.

Pan-cancer analysis of GARS1 expression and infiltrating immune cells

We first performed a pan-cancer analysis of the correlation between *GARS1* expression levels and 24 immune cells (Fig. 7a). The correlation analysis between the expression of *GARS1* and immune cells was analyzed by ssGSEA based on Spearman's R. From the heatmap of the correlation analysis, we found that the expression of *GARS1* was positively associated with Th2 cells across the pan-caner with significant differences except TGCT, KICH, LUSC, CESC and CHOL (Fig. 7b–i). In contrast, pDCs were negatively associated with *GARS1* expression across cancers, with significant differences except for CHOL and UCS (Fig. 7j–q).

Then, we have performed the co-expression of *GARS1*with immune-associated genes in 33 cancer types. The immune associated genes included MHC genes, chemokines, chemokine receptors, immune activation genes and immunosuppressive genes. From the results, we found *GARS1* was associated with the majority of immune-associated genes except CESC, CHOL, LAML, MESO, OV and PAAD ($p < 0.05$) (Fig. 8). We found that

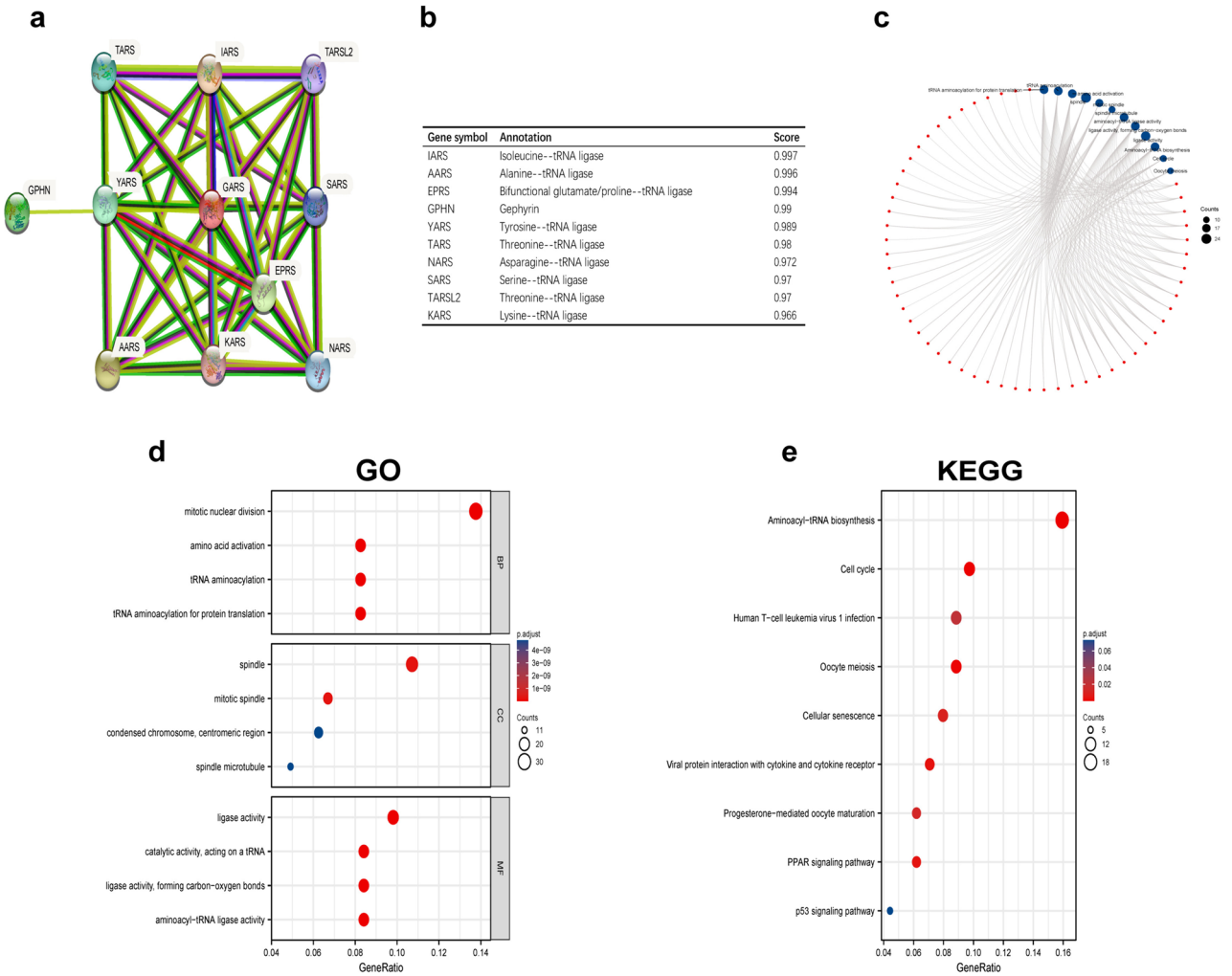

Gene symbol	Annotation	Score
IARS	Isoleucine--tRNA ligase	0.997
AARS	Alanine--tRNA ligase	0.996
EPRS	Bifunctional glutamate/proline--tRNA ligase	0.994
GPHN	Gephyrin	0.99
YARS	Tyrosine--tRNA ligase	0.989
TARS	Threonine--tRNA ligase	0.98
NARS	Asparagine--tRNA ligase	0.972
SARS	Serine--tRNA ligase	0.97
TARSL2	Threonine--tRNA ligase	0.97
KARS	Lysine--tRNA ligase	0.966

Figure 5. (**a**) Protein–protein interaction (PPI) network, (**b**) annotation of *GARS1*-interacting proteins and their co-expression scores, (**c**) Visual network of GO and KEGG analyses, (**d**) GO analysis, and (**e**) KEGG analysis.

MHC genes, chemokines and chemokine receptors were positively associated with *GARS1* especially in BLCA, BRCA, KICH, KIRC, KIRP, LGG, LIHC, PRAD, and UVM (Fig. 8a–c). We also found that immune activation genes were co-expressed with *GARS1* in almost all cancer types (besides CESC, CHOL, DLBC, ESCA, MESO, and SARC). In particular, the immune activation genes PVR, NTSE, ULBP1 and CD276 were widely associated with the expression of *GARS1* (Fig. 8d). In addition, immunosuppressive genes were positively correlated with *GARS1* including TGFB1, TGFBR1, IL10, IL10RB, and CD274 particularly in BLCA, BRCA, KICH, KIRC, KIRP, LIHC, THCA, UCEC and UVM (Fig. 8e).

Regression analyses of GARS1 expression with OS in BLCA

By conducting univariate Cox regression analysis, we found that high *GARS1* expression, lymphovascular invasion, high pathologic grade (stage III&IV) and stage (T, N, and M) were poor predictors of OS events in BLCA patients. Meanwhile, multivariate cox proportional-hazards model analysis showed that higher expression of *GARS1* was an independent factor associated with worse OS (Fig. 9).

Nomogram for predicting OS and validation by calibration

A nomogram was constructed to predict the prognosis of BLCA in specific clinical situations, which integrates the relative clinical characteristics with the OS of BLCA patients. The nomogram assigned a specific point to the clinical situation, and we summed and recorded the total points to evaluate patient outcomes. By matching the total points and absolute axis below, we can determine the probability of survival at 1, 3 and 5 years in BLCA patients (Fig. 10a). The nomogram results showed that *GARS1* expression contributes secondarily to the total points compared with other specific clinical situations which are lower than the T pathologic grade. To validate the results of nomogram, we constructed a calibration model and the plot was close to the ideal curve (45-degree) line, which indicated that the predicted and observed values were consistent (Fig. 10b).

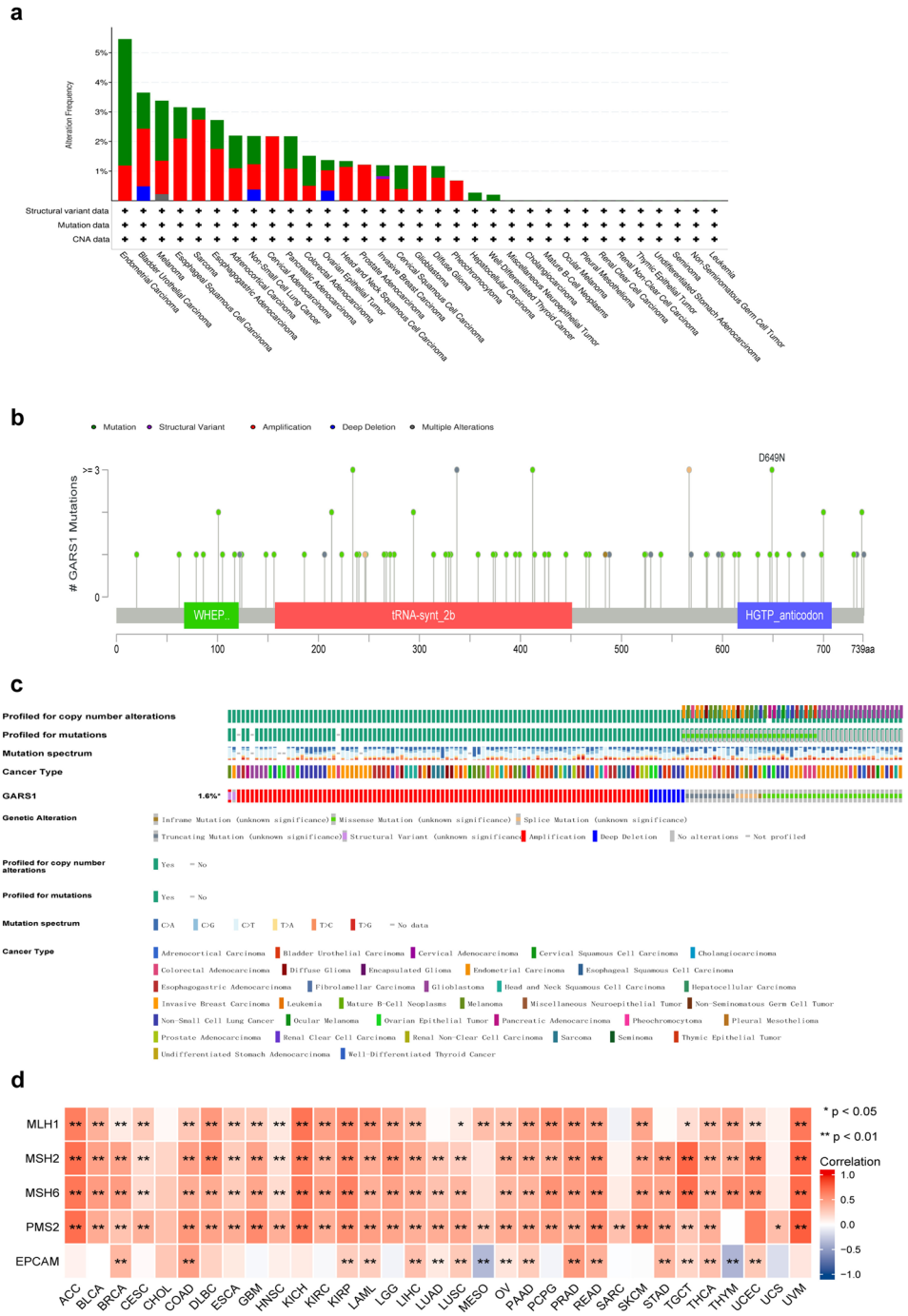

Figure 6. Pan-cancer analysis of *GARS1* genetic features. (**a**) Frequencies of *GARS1* genetic alterations across cancers from TCGA. (**b**) The mutation type and mutation site of *GARS1* from cBioportal. (**c**) Mutation spectrum of *GARS1* across TCGA pan-caner by cBioPortal Oncoprint. (**d**) Association between the expression of *GARS1* and five key MMR genes that indicate mutation levels (MLH1, PMS2, MSH6, EPCAM, MSH2). Correlations were calculated by Pearson's test. p-value. *p < 0.05; **p < 0.01.

GSEA identified GARS1-related signaling pathways in BLCA

Based on the MSigDB Collection enrichment (c2.all.v7.0.symbols.gmt), GSEA was used to identify *GARS1* related signaling pathways between the different *GARS1* expression levels with significant difference in BLCA (adjusted p-value < 0.001 and FDR < 0.005). The eight signaling pathways included formation of the cornified envelope, keratinization, immunoregulatory interactions between a lymphoid and a non-lymphoid cell, CD22 mediated bcr-regulation, KEGG-graft versus host disease, KEGG-antigen processing and presentation, Fcgr-activation, and antigen activates b cell receptor bcr leading to generation of second messengers (Fig. 11).

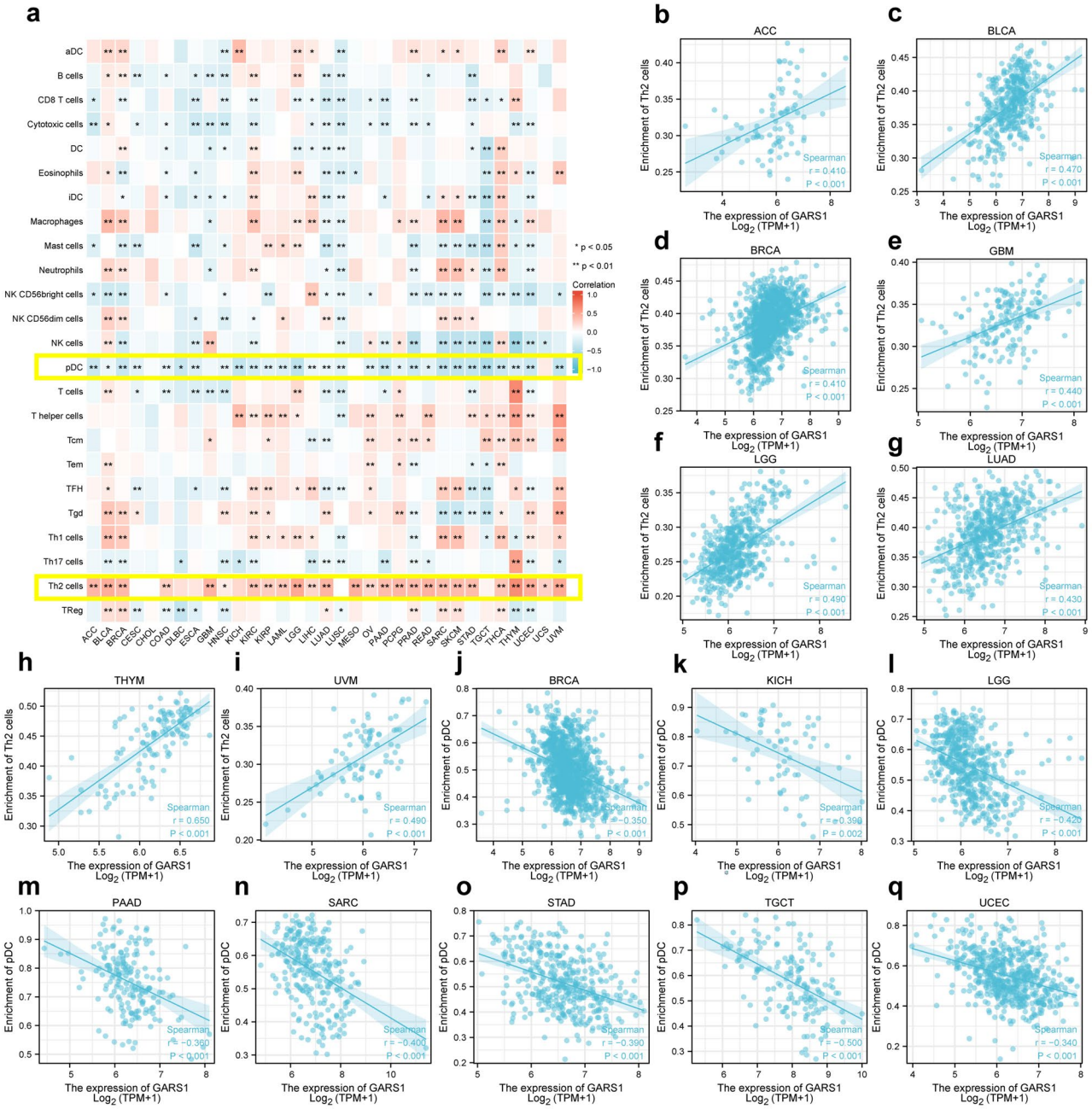

Figure 7. (**a**) Heatmap of the relationship between the different immune cell infiltration levels and *GARS1* expression in various cancers. (**b**–**i**) Positive association of *GARS1* expression and Th2 cells in the heatmap. (**j**–**q**) Negative association of *GARS1* expression with pDCs in various cancers. Correlations were calculated by Pearson's test. p-value. *p < 0.05; **p < 0.01.

Correlation between GARS1 and infiltrating immune cells with specific gene marker in BLCA

The public databases TIMER2 and GEPIA2 were used to further explore the role of *GARS1* expression in the process of immune cell infiltration with various gene markers. We analyzed the correlation between the expression of *GARS1* and immune cell with different markers. From the results, M2 macrophages, TAM, Th1 and T cell exhaustion set markers were greatly associated with the expression of *GARS1* in BLCA patients (Table 1).

DNA methylation status of GARS1 in BLCA

Compared with those in normal tissues, the DNA methylation levels of *GARS1* were significantly lower (Fig. 12a). From the results, we found high-grade tumors with a low methylation status of *GARS1* (Fig. 12b). In addition, historical subtypes of papillary and non- papillary *GARS1* methylation were both lower than those in normal tissues but there was no statistical difference between the two subtypes (Fig. 12c). Through a heatmap from the

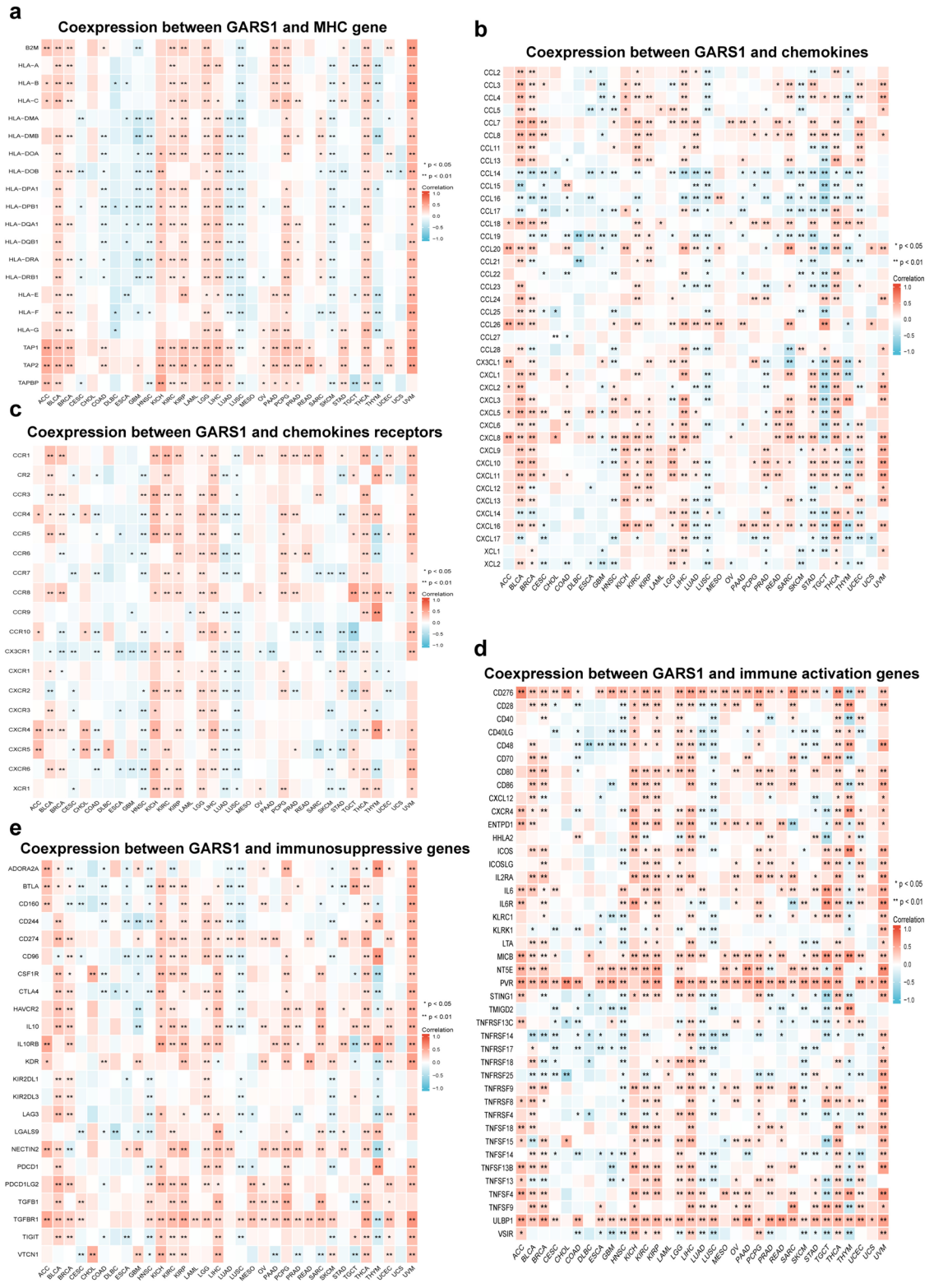

Figure 8. Immune-associated co-expression of *GARS1* across cancers. (**a**) Co-expression of *GARS1* with MHC genes. (**b**) Co-expression between *GARS1* and chemokines. (**c**) Co-expression of *GARS1* with chemokine receptors. (**d**) Co-expression of *GARS1* with immune activation genes. (**e**) Co-expression between *GARS1* and immunosuppressive genes. Correlations were calculated by Pearson's test. p-value. *p < 0.05; **p < 0.01.

a

Characteristics	Total(N)	HR(95% CI) Univariate analysis	P value Univariate analysis
Age	413		
<=70	233	Reference	
>70	180	1.421 (1.063−1.901)	0.018
Gender	413		
Female	109	Reference	
Male	304	0.849 (0.616−1.169)	0.316
T stage	379		
T1&T2	124	Reference	
T3&T4	255	2.199 (1.515−3.193)	<0.001
N stage	369		
N0	239	Reference	
N2&N3&N1	130	2.289 (1.678−3.122)	<0.001
M stage	213		
M0	202	Reference	
M1	11	3.136 (1.503−6.544)	0.002
Pathologic stage	411		
Stage I&Stage II	134	Reference	
Stage III&Stage IV	277	2.310 (1.596−3.342)	<0.001
Subtype	408		
Non−Papillary	275	Reference	
Papillary	133	0.690 (0.488−0.976)	0.036
Lymphovascular invasion	282		
No	130	Reference	
Yes	152	2.294 (1.580−3.328)	<0.001
GARS1	413		
Low	207	Reference	
High	206	1.697 (1.261−2.285)	<0.001

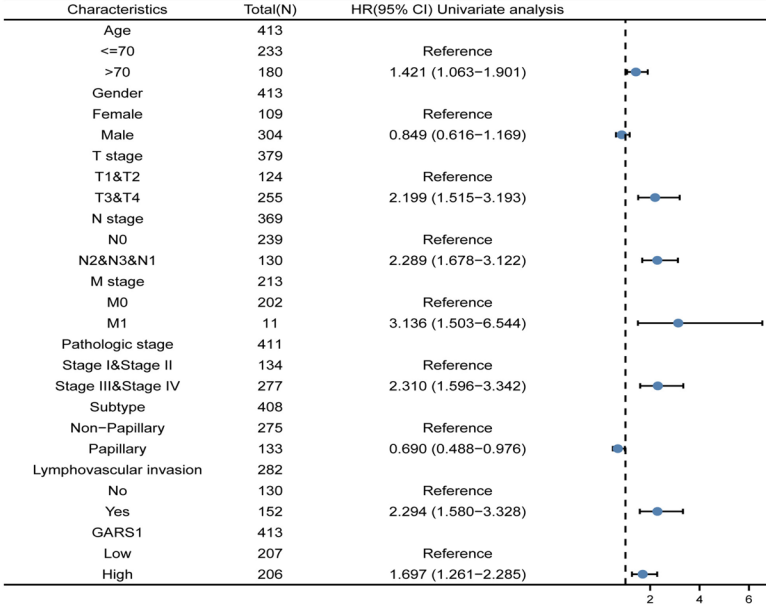

b

Characteristics	Total(N)	HR(95% CI) Multivariate analysis	P value Multivariate analysis
Age	413		
<=70	233		
>70	180	0.988 (0.524−1.862)	0.969
Gender	413		
Female	109		
Male	304		
T stage	379		
T1&T2	124		
T3&T4	255	2.579 (0.568−11.710)	0.22
N stage	369		
N0	239		
N2&N3&N1	130	1.235 (0.581−2.628)	0.583
M stage	213		
M0	202		
M1	11	1.357 (0.390−4.721)	0.632
Pathologic stage	411		
Stage I&Stage II	134		
Stage III&Stage IV	277	0.549 (0.090−3.354)	0.516
Subtype	408		
Non−Papillary	275		
Papillary	133	1.358 (0.660−2.795)	0.407
Lymphovascular invasion	282		
No	130		
Yes	152	2.902 (1.291−6.522)	0.01
GARS1	413		
Low	207		
High	206	1.989 (1.017−3.892)	0.045

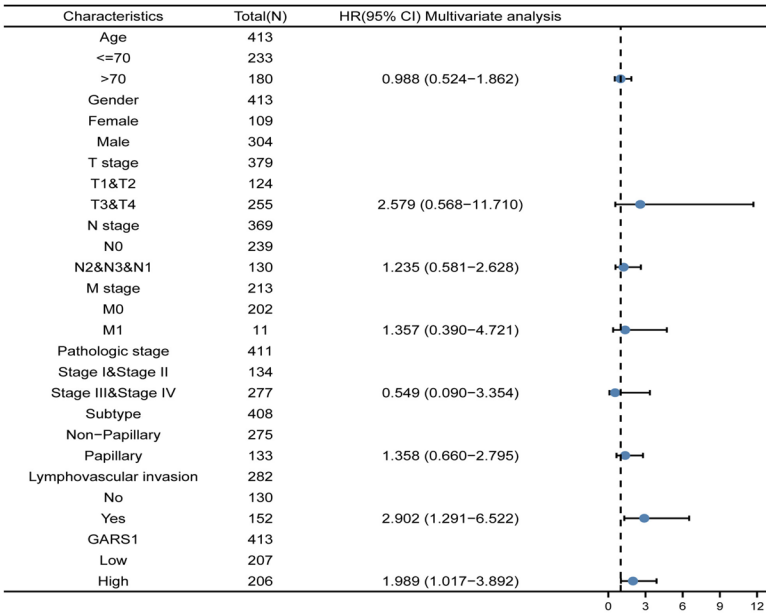

Figure 9. Univariate (**a**) and multivariate (**b**) regression analyses of *GARS1* and other clinicopathologic parameters with OS in BLCA patients.

MethSurv database, we found that CpG sites of *GARS1*, including cg09351960, cg20948778, cg08712082, and cg18770728, showed higher methylation levels in BLCA (Fig. 12d).

GARS1 expression promotes BLCA cells proliferation, and metastasis and inhabits apoptosis in vitro

The expression level of *GARS1* was remarkably higher in T24T, and RT4 cells than in human bladder epithelium immortalized cells (SV) by RT-qPCR analysis, and the expression of *GARS1* was relatively low in the EJ and T24 cell lines (Fig. 13a). To explore the potential function of *GARS1* in BLCA, we constructed *GARS1*-overexpressing BLCA cells in EJ and T24 cells by transfecting the *GARS1* overexpression plasmid into *GARS1*-depleted BLCA cells in T24T and RT4 cells by transfection with GARS shRNA (Fig. 13b–e). We further used the CCK-8 assay to evaluate the proliferation ability of cell lines in vitro. Experiments showed that the OD values were higher in the *GARS1* overexpressing groups than in the control groups, with significant differences at the end of the experiments in the EJ and T24 cell lines (Fig. 13f,g). We also found that OD values were lower in the *GARS1* depletion groups in T24 and RT4 (Fig. 13h,i). Experiments showed us that overexpression improved the viability of EJ and T24 cells (Fig. 13j,k), and the depletion of GARS inhibited RT4 and T24T cell viability (Fig. 13l,m). We used

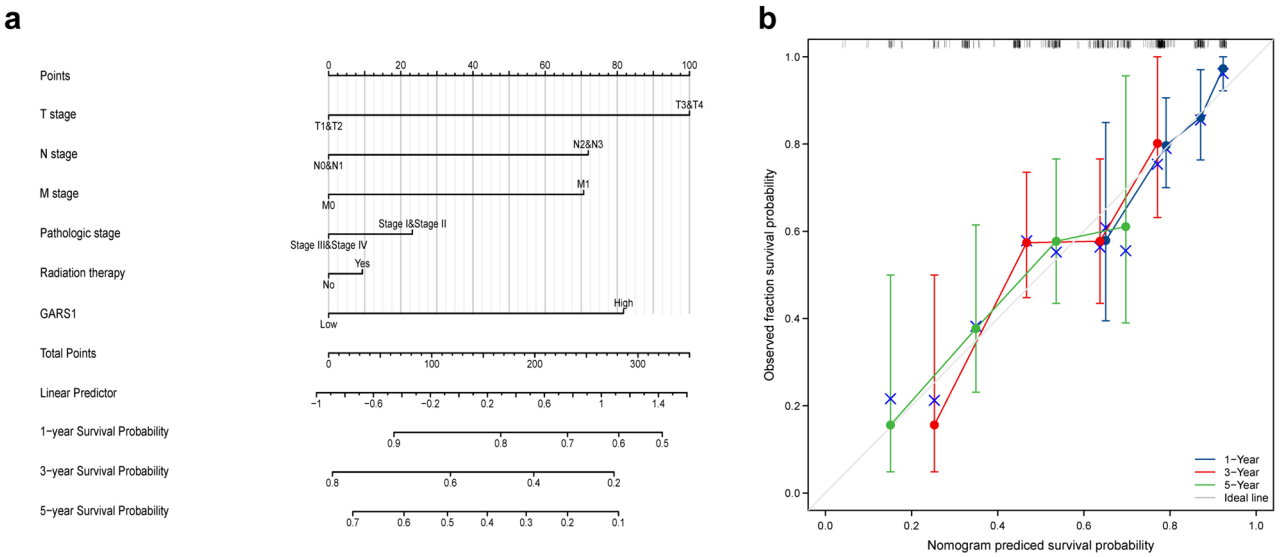

Figure 10. The relationship of *GARS1* expression with other clinical factors and overall survival (OS). (**a**) Nomogram for predicting the probability of 1-, 3-, and 5-year OS for BLCA patients; (**b**) calibration plot of the nomogram for predicting the OS likelihood.

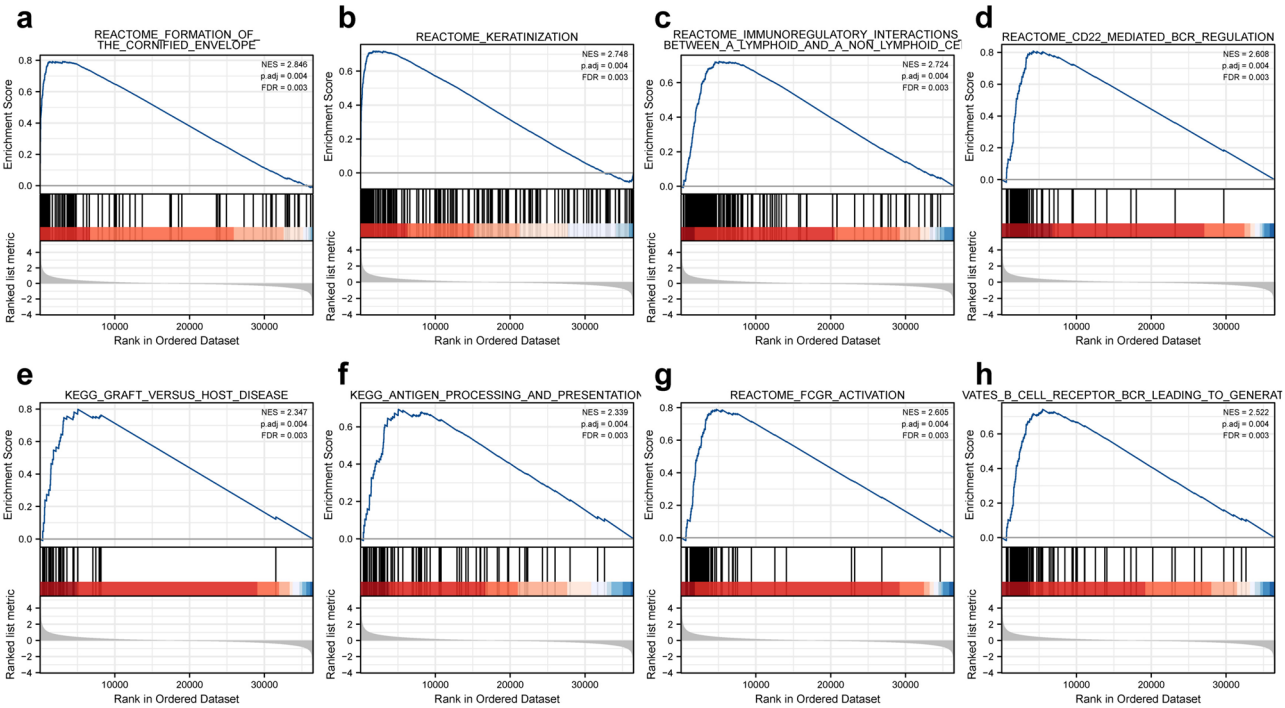

Figure 11. Enrichment plots from GSEA. Several pathways were differentially enriched in BLCA patients according to different *GARS1* expression levels; (**a**) formation of the cornified envelope; (**b**) keratinization; (**c**) immunoregulatory interactions between a lymphoid and a non-lymphoid cell; (**d**) CD22 mediated bcr-regulation; (**e**) KEGG-graft versus host disease; (**f**) KEGG-antigen processing and presentation; (**g**) Fcgr-activation; (**h**) antigen activates b cell receptor bcr leading to generation of second messengers; *ES* enrichment score, *NES* normalized enrichment score, *ADJ p-Val* adjusted p-value, *FDR* false discovery rate.

Transwell assays to further confirm the function of *GARS1* in BLCA metastasis. In EJ and T24 cells, the number of migrated and invaded cell in the overexpression groups were higher than those in the NC group (Fig. 14a,b). Meanwhile, in RT4 and T24T cells, the sh-*GARS1* groups migrated and invaded cell numbers were dramatically less than those in the shNC group (Fig. 14c,d). The results indicated that silencing *GARS1* could damage migration and invasion of BLCA cells. Conversely, overexpressing *GARS1* improves the ability to migrate and invade. Annexin V-PE/7-AAD double staining was further employed for apoptosis examination combined with flow

Cell type	Gene marker	None Cor	p	Purity Cor	p	Tumor R	p	Normal R	p
B cell	CD19	0.118	*	0.01	0.85	−0.025	0.62	0.48	*
	CD20 (KRT20)	−0.137	**	−0.061	0.246	−0.055	0.27	0.21	0.4
	CD38	0.318	***	0.213	***	0.062	0.21	0.42	0.073
CD8+ T cell	CD8A	0.233	***	0.108	*	0.096	0.055	0.21	0.38
	CD8B	0.192	***	0.11	*	0.41	*	0.28	0.25
Tfh	BCL6	−0.22	***	−0.195	***	−0.16	**	−0.36	0.13
	ICOS	0.252	***	0.124	*	0.077	0.12	0.53	*
	CXCR5	0.09	0.0708	−0.07	0.183	0.1	*	0.45	0.056
Th1	T-bet (TBX21)	0.199	***	0.064	0.22	0.08	0.11	0.36	0.13
	STAT4	0.213	***	0.081	0.119	0.076	0.13	0.27	0.27
	IL12RB2	0.369	***	0.305	***	0.079	0.11	0.31	0.2
	WSX1 (IL27RA)	0.357	***	0.302	***	0.17	***	0.46	*
	STAT1	0.369	***	0.293	***	0.049	0.32	−0.051	0.84
	IFN-γ (IFNG)	0.23	***	0.138	**	0.13	**	−0.19	0.43
	TNF-α (TNF)	0.225	***	0.145	**	0.11	*	0.064	0.79
Th2	GATA3	−0.244	***	−0.174	***	−0.0075	0.88	−0.16	0.52
	CCR3	0.142	**	0.108	0.0386	0.1	*	0.27	0.27
	STAT6	−0.198	***	−0.171	***	−0.25	***	−0.7	***
	STAT5A	0	0.999	−0.094	0.0702	−0.089	0.075	−0.37	0.12
Th9	TGFBR2	0.176	***	0.116	*	0.037	0.45	−0.53	*
	IRF4	0.171	***	−0.001	0.983	−0.015	0.77	0.36	0.13
	PU.1 (SPI1)	0.259	***	0.127	*	0.17	***	0.24	0.31
Th17	STAT3	0.272	***	0.208	***	−0.098	*	−0.33	0.17
	IL-21R	0.247	***	0.114	*	0.051	0.31	0.48	*
	IL-23R	−0.068	0.172	−0.123	*	−0.069	0.17	0.22	0.36
	IL-17A	−0.0029	0.553	−0.038	0.462	−0.0069	0.89	0.021	0.93
Th22	CCR10	−0.059	0.236	−0.07	0.181	0.019	0.71	0.062	0.8
	AHR	−0.033	0.51	0.015	0.774	0.073	0.14	−0.25	0.3
Treg	FOXP3	0.255	***	0.145	**	0.084	0.093	0.51	*
	CD25 (IL2RA)	0.351	***	0.264	***	0.14	**	0.21	0.39
	CCR8	0.275	***	0.174	***	−0.0069	0.89	0.4	0.093
T cell exhaustion	PD-1 (PDCD1)	0.195	***	0.053	0.313	0.065	0.19	0.44	0.061
	CTLA4	0.223	***	0.084	0.106	0.15	**	0.48	*
	LAG3	0.302	***	0.193	***	0.18	***	0.34	0.15
	TIM-3 (HAVCR2)	0.34	***	0.235	***	0.18	***	0.14	0.58
Macrophage	CD68	0.226	***	0.13	*	0.078	0.12	0.2	0.42
	CD11b (ITGAM)	0.29	***	0.19	***	0.004	0.94	−0.15	0.55
M1	INOS (NOS2)	0.097	0.0512	0.08	0.127	−8.80E−05	1	6.80E−02	0.78
	IRF5	−0.128	**	−0.135	**	−0.045	0.36	0.18	0.47
	COX2 (PTGS2)	0.057	0.249	0.012	0.816	−0.0043	0.93	−0.19	0.44
M2	CD16	0.393	***	0.313	***	0.15	**	0.0035	0.99
	ARG1	−0.046	0.354	0.013	0.8	−0.014	0.78	0.47	*
	MRC1	0.354	***	0.277	***	0.12	*	−0.32	0.19
	MS4A4A	0.358	***	0.268	***	0.22	***	−0.3	0.21
TAM	CCL2	0.259	***	0.143	**	0.18	**	−0.094	0.7
	CD80	0.358	***	0.271	***	0.15	**	0.34	0.16
	CD86	0.342	***	0.251	***	0.2	***	0.24	0.33
	CCR5	0.269	***	0.146	**	0.095	0.055	0.34	0.15
Monocyte	CD14	0.327	***	0.226	***	0.18	***	0.0061	0.98
	CD16 (FCGR3B)	0.219	***	0.153	**	0.011	0.83	0.059	0.81
	CD115 (CSF1R)	0.293	***	0.174	***	0.18	***	−0.18	0.47
Neutrophil	CD66b (CEACAM8)	0.001	0.987	0.03	0.57	−0.052	0.29	0.2	0.41
	CD15 (FUT4)	0.302	***	0.248	***	0.018	0.72	−0.32	0.18
	CD11b (ITGAM)	0.29	***	0.19	***	0.004	0.94	−0.15	0.55

Continued

Cell type	Gene marker	None Cor	p	Purity Cor	p	Tumor R	p	Normal R	p
Natural killer cell	XCL1	0.052	0.293	0.064	0.221	0.068	0.17	0.59	0.13
	CD7	0.192	***	0.041	0.429	0.096	0.053	0.46	*
	KIR3DL1	0.119	0.0162	0.037	0.48	0.019	0.71	0.55	*
Dendritic cell	CD1C (BDCA-1)	−0.055	0.271	−0.17	**	−0.022	0.66	0.41	0.085
	CD141 (THBD)	0.143	**	0.08	0.123	0.016	0.75	0.071	0.77
	CD11c (ITGAX)	0.321	***	0.203	***	0.079	0.11	0.21	0.38

Table 1. Correlation analysis between *GARS1* and markers of immune cells in BLCA patients in TIMER2 and GEPIA2. *BLCA* bladder urothelial carcinoma, *Tfh* follicular helper T cell, *Th* T helper cell, *Treg* regulatory T cell, *TAM* tumor-associated macrophage. None, Correlation without adjustment; Purity, correlation conditioned on tumor purity; Tumor, correlation analysis in tumor tissue of TCGA; Normal, correlation analysis in normal tissue of TCGA. Cor, R value of Pearman's correlation *p < 0.05; **p < 0.01; ***p < 0.001.

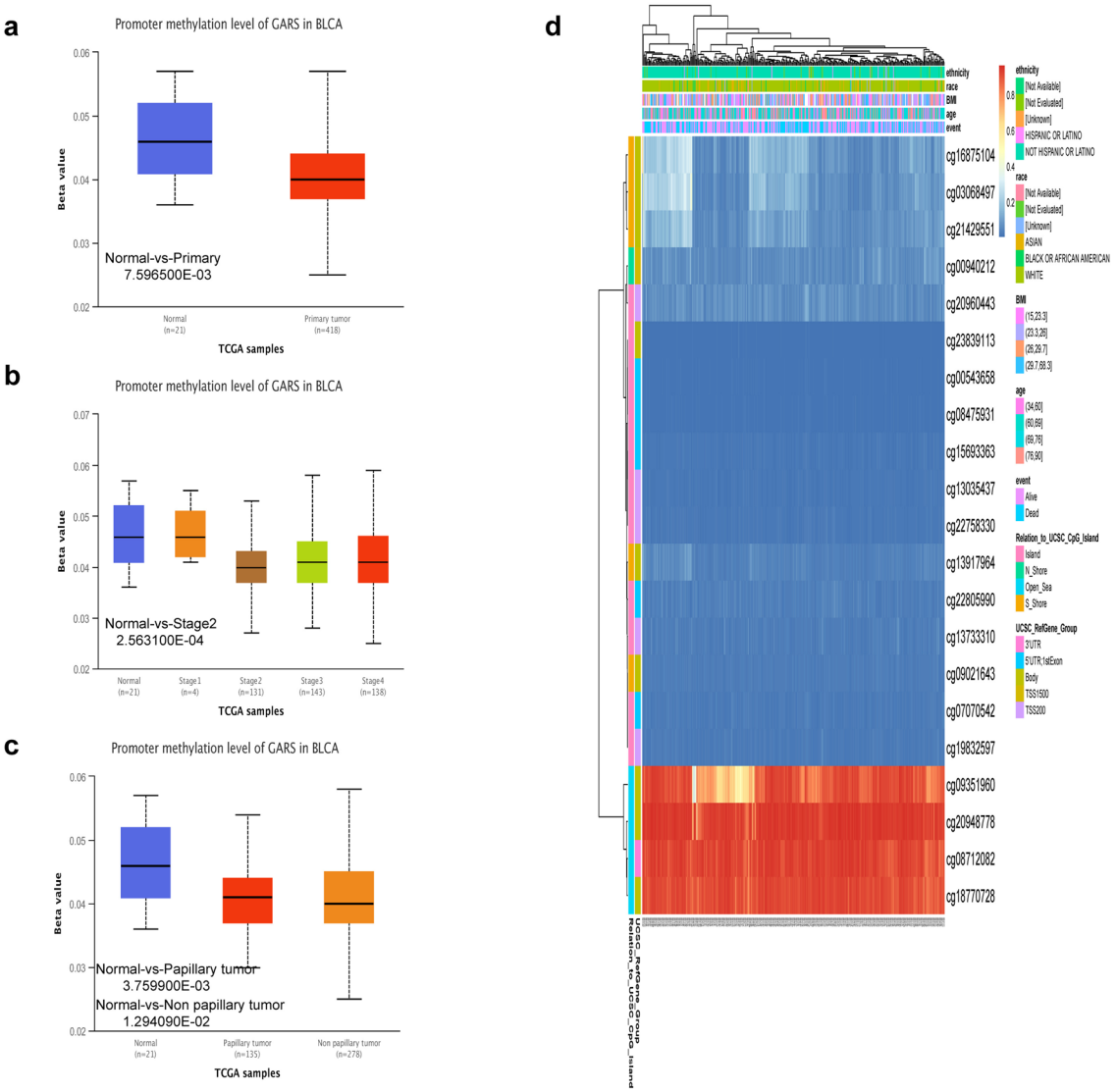

Figure 12. DNA methylation levels of GARS in BLCA. (**a**) Promoter methylation level of GARS in normal tissues and primary tumor tissues by the UALCAN database. (**b**) Promoter methylation level of GARS in BLCA tissues of various tumor stages. (**c**) Promoter methylation level of GARS in BLCA tissues by historical subtypes. (**d**) The heatmap of DNA methylation at CpG sites in the GARS gene by the MethSurv database.

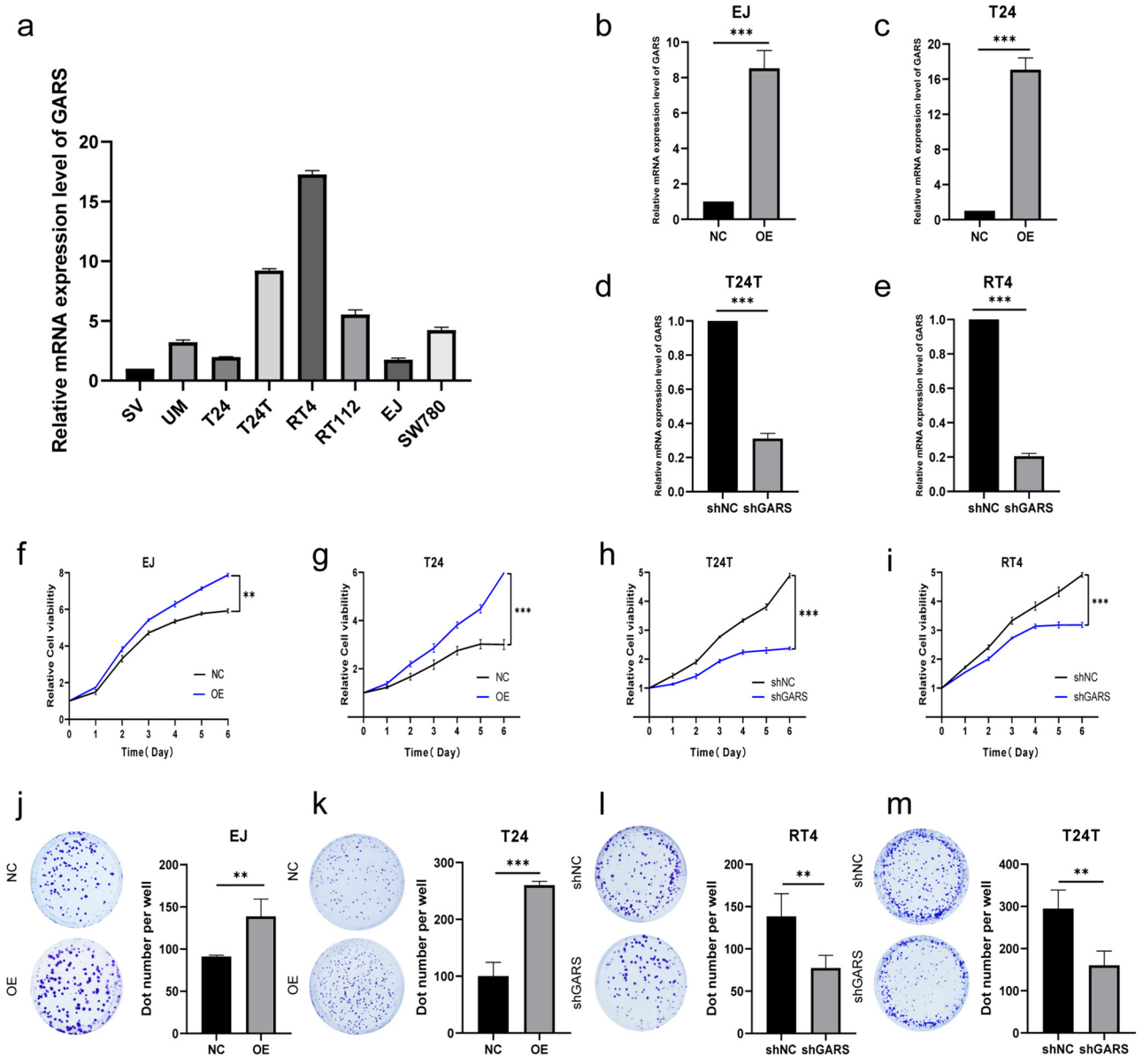

Figure 13. (**a**) mRNA level of *GARS1* in human bladder epithelium immortalized Cells (SV) and seven BLCA cell lines, including UM, T24, T24T, RT4, RT112, EJ, and SW780. (**b**–**e**) The mRNA level of *GARS1* in EJ, T24, T24T, and RT4 cells after *GARS1* overexpression or depletion. (**f**–**g**) The viability of EJ and T24 cells after *GARS1* overexpression. (**h**,**i**) The viability of T24T and RT4 cells after *GARS1* depletion. (**j**,**k**) Images exhibited the colony formation and the colony quantification number. *p < 0.05, **p < 0.01, ***p < 0.001, ****p < 0.0001.

cytometry. In EJ and T24 cells, the apoptotic rates of the *GARS1*-overexpressing groups were lower than those of the control groups (Fig. 14e,f). In contrast, the *GARS1* apoptotic rates of the depletion groups were higher than those of the control groups (Fig. 14g,h). Overall, the expression of *GARS1* improves the ability of BLCA cells to proliferate, metastasize, and inhibit apoptosis in vitro.

Discussion

Some studies illustrated that *GARS1* missense mutations were associated with Charcot–Marie–Tooth (CMT) subtype 2D (CMT-2D) and distal hereditary motor neuropathy-V (dHMN-V). CMT-2D and dHMN-V are peripheral nervous system hereditary diseases[48,49]. One study found that extracellular vesicles from macrophages display *GARS1* and show anticancer activity[20], and one study explored the function of secreted *GARS1* in defense against ERK-activated tumorigenesis[50]. Increasing evidence shows that the multiple functions of *GARS1* are systematic factors and are controlled through sophisticated mechanisms in respond to different cellular stimuli in the progression of cancers[19,51–53]. However, the specific functions of *GARS1* have not been extensively studied across cancers. Therefore, it is urgent to explore the function of *GARS1* in the progression of tumors through multiple omics integrative pan-cancer analysis.

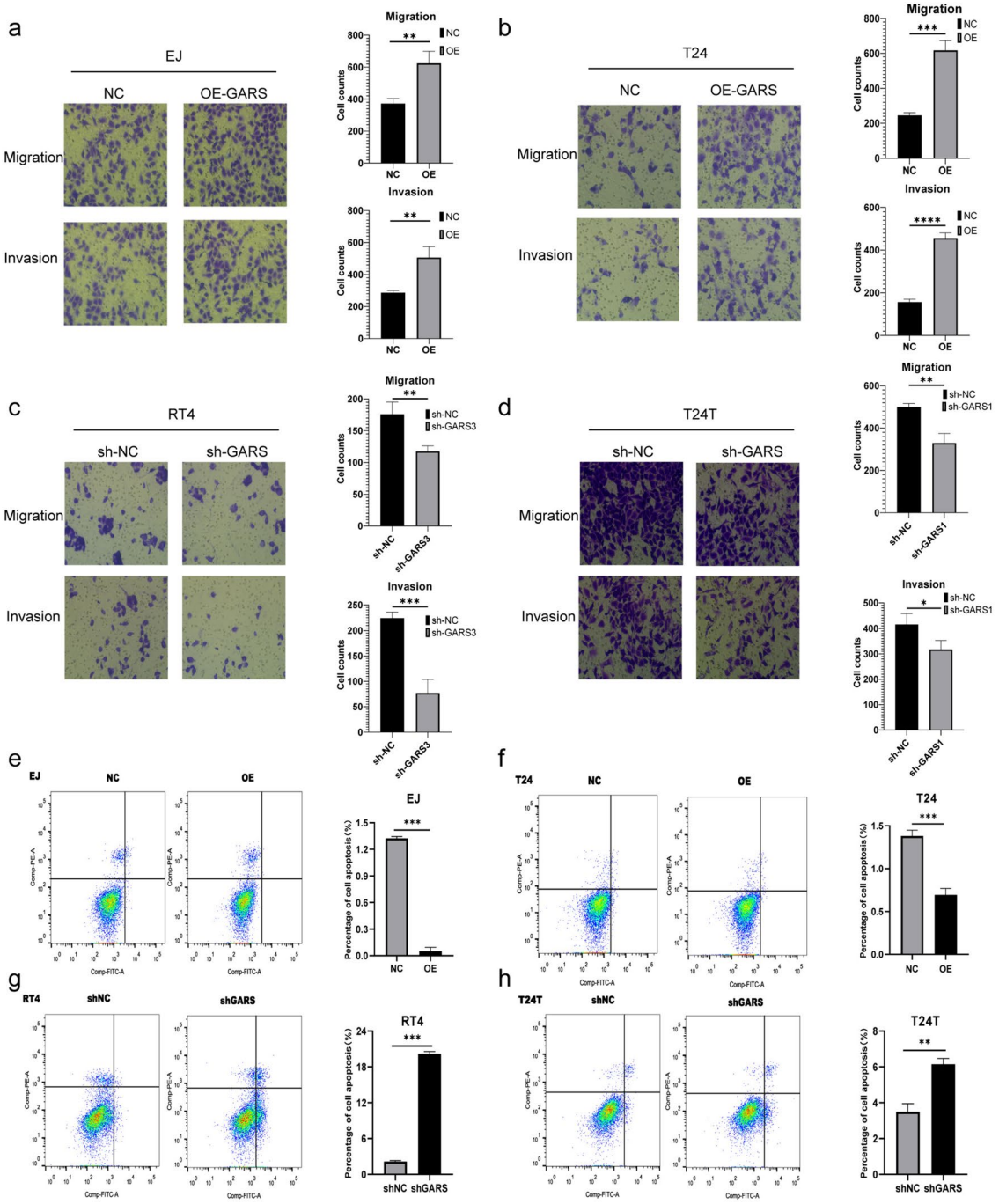

Figure 14. Images and number of migrated cells and invaded cells of (**a**) EJ, (**b**) T24, (**c**) RT4, (**d**) T24T. Cell apoptosis of (**e**) EJ, (**f**) T24, (**g**) RT4, and (**h**) T24T cells detected by flow cytometry (magnification ×200). $^{**}p < 0.001$, $^{***}p < 0.0001$.

In our study, we explored the expression pattern, and prognostic and diagnostic value of *GARS1* in across cancers through Kaplan–Meier Plotter, ROC curves and multiple databases including TCGA, GTEx, CCLE, and HPA. From the results, we found that *GARS1* expression level was higher than in 12 tumors compared with the normal tissues, including BLCA, COAD, DLBC, ESCA, LIHC, PAAD, READ, STAD, TGCT, THYM, UCEC and UCS, while the expression level of *GARS1* in LAML was lower than that in normal tissue (Fig. 1). Further investigation of *GARS1* protein expression through the HPA and CPTAC databases revealed that BLCA, COAD, LIHC, TGCT, RCC, OV, LUAD, and UCEC had higher expression of *GARS1* total protein (Fig. 2). The differences in *GARS1* gene and protein expression in various tumor types reflect the underlying functions and mechanisms of tumor progression and development. Then, we found that *GARS1* expression was a high-risk indicator poor prognosis in ACC, BLCA, BRCA, HNSC, KICH, KIRP, LGG, LIHC, LUAD, MESO, PAAD, SARC, UCEC, and UVM (Fig. 3). The ROC curve also indicated that the expression of *GARS1* was highly accurate in the diagnosis

of BLCA, BRCA, COAD, ESCA, KIRP, READ, STAD, TGCT, UCEC, and UCS (Fig. 4). These results indicate that *GARS1* is a diagnostic and prognostic biomarker for some types tumors. We also constructed a genetic features atlas, a PPI network, and GO and KEGG analyses of *GARS1* to comprehensively understand the functional mechanisms of *GARS1* (Figs. 5, 6).

The tumor microenvironment (TME) contains various types of cells, including immune cells, stromal cells, cancer-associated fibroblasts and endothelial cells which constitute vital elements of tumors. Increasing evidence has revealed that the TME influences the therapeutic response and clinical outcome[54,55]. From the results, the expression of *GARS1* was positively associated with Th2 cells across all cancers except TGCT, KICH, LUSC, CESC and CHOL. In contrast, pDCs were negatively associated with *GARS1*, except for CHOL and UCS (Figs. 7, 8). Our results proved that *GARS1* has a positive relationship with Th2 cell infiltration, which may disrupt the Th1/Th2 balance and contribute to tumor progression and immune system weakening[56]. Then, we performed co-expression analysis of *GARS1* expression with immune-associated genes across cancers. We found MHC genes, chemokines and chemokine receptors were positively associated with *GARS1* especially in BLCA, BRCA, KICH, KIRC, KIRP, LGG, LIHC, PRAD, UVM and immune activation genes were co-expressed with *GARS1* in almost all cancer types (except for CESC, CHOL, DLBC, ESCA, MESO, and SARC). In particular, the immune activation genes PVR, NTSE, ULBP1 and CD276 were widely associated with the expression of *GARS1*. Surprisingly, immunosuppressive genes were positively correlated with *GARS1*, including TGFB1, TGFBR1, IL10, IL10RB, and CD274. Our results show that *GARS1* might play an essential role in the tumor microenvironment, especially in immunosuppression-relative genes, The high expression of *GARS1* associated with immunosuppression suggests that *GARS1* might be a potential target for immunotherapy.

Furthermore, we tested and verified *GARS1* as a novel prognostic and immunological biomarker in BLCA. The multivariate Cox proportional hazards model[57] showed that the higher expression of *GARS1* was an the independent factor associated with worse OS (Fig. 9). A nomogram and calibration curve were constructed to predict the prognosis of BLCA in specific clinical situations, integrating the relative clinical characteristics with the OS of BLCA patients[58]. The results showed that *GARS1* expression predicted poor survival in BLCA patients and accurately predicted 1-, 3-, and 5-year OS in BLCA patients to screen and identify high-risk patients (Fig. 10). From the DNA methylation atlas, BLCA tissues expressed a low methylation status as well as a high grade of tumors, which indicated that *GARS1* methylation changes may lead to BLCA progression (Fig. 12). T-cell exhaustion is the T-cell dysfunction that occurs in many chronic cancers, and exhaustion prevents optimal control of infection and tumors[59]. Moreover, we found that M2 macrophages, TAMs, Th1 and T cell exhaustion sets marking were greatly associated with the expression of *GARS1* in BLCA patients (Table 1). *GARS1* may be a potential target in adjusting the tumor microenvironment. In vitro experiments showed that *GARS1* is a potential oncogene promotes BLCA cells proliferation, metastasis and inhabits apoptosis (Figs. 13, 14).

We demonstrate that *GARS1* can serve as a novel prognostic and immunological biomarker through multiple omics integrative pan-cancer analysis, especially in BLCA. *GARS1* could serve as an oncogene which was validated by in vitro experiments. Immune infiltration was significantly associated with high *GARS1* expression, and we constructed immune-association heatmaps to show that *GARS1* correlated with specific immune-related genes. Our research was the first to illustrate the potential functional role of *GARS1*, which might guide us to a novel biomarker that influences T-cell exhaustion infiltration and immunosuppressive gene expression. In vitro experiments validated that *GARS1* expression promotes BLCA cell proliferation and metastasis and inhibits apoptosis. Our results show that *GARS1* is a valuable diagnostic, prognostic biomarker and a potential target for immunotherapy in BLCA.

This study developed a pan-cancer biomarker related to tumor immunity to predict tumor survival and immune efficacy, with a particular focus on bladder cancer. Unfortunately, we have not yet collected data on bladder cancer cases from our center for external validation of the model's accuracy. In the next phase of our research, we will utilize our own data on bladder cancer to assess the discrimination and conformity of the GARS1 model. As tumor immunotherapy continues to advance, the mechanisms by which GARS1 influences immune infiltration and the tumor microenvironment will be explored further, particularly in relation to its interaction with ICI and bladder cancer.

Conclusions

GARS1 can serve as a novel prognostic and immunological biomarker through multiple omics integrative pan-cancers analysis especially in BLCA. The expression of *GARS1* was positively correlated with immune infiltration which indicated that *GARS1* may be related to the tumor immune microenvironment. *GARS1* functions in vitro were validated by experiments.

Data availability

The cancer genome database (TCGA) (https://portal.gdc.cancer.gov); GTEx (https://commonfund.nih.gov/GTEx); CCLE database (https://portals.broadinstitute.org/ccle/); Gene Expression Profiling Interactive Analysis 2 (GEPIA2) (http://gepia2.cancer-pku.cn/#index); The Human Protein Atlas (HPA) (https://www.proteinatlas.org/); UALCAN (http://ualcan.path.uab.edu/analysis-prot.html); Search Tool for the Retrieval of Interacting Genes/Proteins (STRING) website (https://cn.string-db.org/); MethSurv (https://biit.cs.ut.ee/methsurv/); All the databases used in our study are publicly available/open-access.

Received: 6 April 2024; Accepted: 12 August 2024
Published online: 16 August 2024

References

1. Sahin, T. K., Rizzo, A., Aksoy, S. & Guven, D. C. Prognostic significance of the Royal Marsden Hospital (RMH) score in patients with cancer: A systematic review and meta-analysis. *Cancers (Basel)* **16**(10), 1835 (2024).
2. Rizzo, A., Mollica, V. & Massari, F. Expression of programmed cell death ligand 1 as a predictive biomarker in metastatic urothelial carcinoma patients treated with first-line immune checkpoint inhibitors versus chemotherapy: A systematic review and meta-analysis. *Eur. Urol. Focus* **8**(1), 152–159 (2022).
3. Jain, R. K. *et al.* Immunotherapy advances in urothelial carcinoma. *Curr. Treat. Options Oncol.* **19**(12), 79 (2018).
4. Rosenberg, J. E. *et al.* Atezolizumab in patients with locally advanced and metastatic urothelial carcinoma who have progressed following treatment with platinum-based chemotherapy: A single-arm, multicentre, phase 2 trial. *Lancet* **387**(10031), 1909–1920 (2016).
5. Rizzo, A. *et al.* Hypertransaminasemia in cancer patients receiving immunotherapy and immune-based combinations: The MOUSEION-05 study. *Cancer Immunol. Immunother.* **72**(6), 1381–1394 (2023).
6. Dall'Olio, F. G. *et al.* Immortal time bias in the association between toxicity and response for immune checkpoint inhibitors: A meta-analysis. *Immunotherapy* **13**(3), 257–270 (2021).
7. Suzman, D. L. *et al.* FDA approval summary: Atezolizumab or pembrolizumab for the treatment of patients with advanced urothelial carcinoma ineligible for cisplatin-containing chemotherapy. *Oncologist* **24**(4), 563–569 (2019).
8. Stühler, V. *et al.* Molecular predictors of response to PD-1/PD-L1 inhibition in urothelial cancer. *World J. Urol.* **37**(9), 1773–1784 (2019).
9. Guven, D. C. *et al.* The association between albumin levels and survival in patients treated with immune checkpoint inhibitors: A systematic review and meta-analysis. *Front. Mol. Biosci.* **9**, 1039121 (2022).
10. Kamoun, A. *et al.* A consensus molecular classification of muscle-invasive bladder cancer. *Eur. Urol.* **77**(4), 420–433 (2020).
11. Srinivasan, G., James, C. M. & Krzycki, J. A. Pyrrolysine encoded by UAG in Archaea: Charging of a UAG-decoding specialized tRNA. *Science (New York, NY)* **296**(5572), 1459–1462 (2002).
12. Sauerwald, A. *et al.* RNA-dependent cysteine biosynthesis in archaea. *Science (New York, NY)* **307**(5717), 1969–1972 (2005).
13. Eriani, G., Delarue, M., Poch, O., Gangloff, J. & Moras, D. Partition of tRNA synthetases into two classes based on mutually exclusive sets of sequence motifs. *Nature* **347**(6289), 203–206 (1990).
14. Delarue, M. & Moras, D. The aminoacyl-tRNA synthetase family: Modules at work. *BioEssays* **15**(10), 675–687 (1993).
15. Guo, M., Yang, X. L. & Schimmel, P. New functions of aminoacyl-tRNA synthetases beyond translation. *Nat. Rev. Mol. Cell Biol.* **11**(9), 668–674 (2010).
16. Freist, W., Logan, D. T. & Gauss, D. H. Glycyl-tRNA synthetase. *Biol. Chem. Hoppe-Seyler* **377**(6), 343–356 (1996).
17. Mazauric, M. H. *et al.* An example of non-conservation of oligomeric structure in prokaryotic aminoacyl-tRNA synthetases. Biochemical and structural properties of glycyl-tRNA synthetase from *Thermus thermophilus*. *Eur. J. Biochem.* **241**(3), 814–826 (1996).
18. Silvera, D., Formenti, S. C. & Schneider, R. J. Translational control in cancer. *Nat. Rev. Cancer* **10**(4), 254–266 (2010).
19. Kim, S., You, S. & Hwang, D. Aminoacyl-tRNA synthetases and tumorigenesis: More than housekeeping. *Nat. Rev. Cancer* **11**(10), 708–718 (2011).
20. Goughnour, P. C. *et al.* Extracellular vesicles derived from macrophages display glycyl-tRNA synthetase 1 and exhibit anti-cancer activity. *J. Extracell. Vesicles* **10**(1), e12029 (2020).
21. Wu, T. & Dai, Y. Tumor microenvironment and therapeutic response. *Cancer Lett.* **387**, 61–68 (2017).
22. Bindea, G. *et al.* Spatiotemporal dynamics of intratumoral immune cells reveal the immune landscape in human cancer. *Immunity* **39**(4), 782–795 (2013).
23. Lee, K. H. *et al.* The prognostic and predictive value of tumor-infiltrating lymphocytes and hematologic parameters in patients with breast cancer. *BMC Cancer* **18**(1), 938 (2018).
24. Lee, N., Zakka, L. R., Mihm, M. C. Jr. & Schatton, T. Tumour-infiltrating lymphocytes in melanoma prognosis and cancer immunotherapy. *Pathology* **48**(2), 177–187 (2016).
25. Topalian, S. L., Drake, C. G. & Pardoll, D. M. Immune checkpoint blockade: A common denominator approach to cancer therapy. *Cancer Cell* **27**(4), 450–461 (2015).
26. Gordon, S. R. *et al.* PD-1 expression by tumour-associated macrophages inhibits phagocytosis and tumour immunity. *Nature* **545**(7655), 495–499 (2017).
27. Pai, C. S. *et al.* Tumor-conditional anti-CTLA4 uncouples antitumor efficacy from immunotherapy-related toxicity. *J. Clin. Investig.* **129**(1), 349–363 (2019).
28. Sharpe, A. H. & Pauken, K. E. The diverse functions of the PD1 inhibitory pathway. *Nat. Rev. Immunol.* **18**(3), 153–167 (2018).
29. Riley, R. S., June, C. H., Langer, R. & Mitchell, M. J. Delivery technologies for cancer immunotherapy. *Nat. Rev. Drug Discov.* **18**(3), 175–196 (2019).
30. Tomczak, K., Czerwińska, P. & Wiznerowicz, M. The Cancer Genome Atlas (TCGA): An immeasurable source of knowledge. *Contemp. Oncol. (Poznan, Poland)* **19**(1a), A68-77 (2015).
31. GTEx Consortium. The Genotype-Tissue Expression (GTEx) project. *Nat. Genet.* **45**(6), 580–585 (2013).
32. Barretina, J. *et al.* The Cancer Cell Line Encyclopedia enables predictive modelling of anticancer drug sensitivity. *Nature* **483**(7391), 603–607 (2012).
33. Tang, Z., Kang, B., Li, C., Chen, T. & Zhang, Z. GEPIA2: An enhanced web server for large-scale expression profiling and interactive analysis. *Nucleic Acids Res.* **47**(W1), W556–W560 (2019).
34. Nusinow, D. P. *et al.* Quantitative proteomics of the cancer cell line encyclopedia. *Cell* **180**(2), 387-402.e16 (2020).
35. Colwill, K. & Gräslund, S. A roadmap to generate renewable protein binders to the human proteome. *Nat. Methods* **8**(7), 551–558 (2011).
36. Chandrashekar, D. S. *et al.* UALCAN: A portal for facilitating tumor subgroup gene expression and survival analyses. *Neoplasia (New York, NY)* **19**(8), 649–658 (2017).
37. Wang, S. *et al.* UCSCXenaShiny: An R/CRAN package for interactive analysis of UCSC Xena data. *Bioinformatics (Oxford, England)* **38**(2), 527–529 (2021).
38. Gao, J. *et al.* Integrative analysis of complex cancer genomics and clinical profiles using the cBioPortal. *Sci. Signal.* **6**(269), pl1 (2013).
39. Modhukur, V. *et al.* MethSurv: A web tool to perform multivariable survival analysis using DNA methylation data. *Epigenomics* **10**(3), 277–288 (2018).
40. Fan, Y. *et al.* Exosomal PD-L1 retains immunosuppressive activity and is associated with gastric cancer prognosis. *Ann. Surg. Oncol.* **26**(11), 3745–3755 (2019).
41. Kanehisa, M., Furumichi, M., Tanabe, M., Sato, Y. & Morishima, K. KEGG: New perspectives on genomes, pathways, diseases and drugs. *Nucleic Acids Res.* **45**(D1), D353–D361 (2017).
42. Kanehisa, M. & Goto, S. KEGG: Kyoto encyclopedia of genes and genomes. *Nucleic Acids Res.* **28**(1), 27–30 (2000).
43. Kanehisa, M. Toward understanding the origin and evolution of cellular organisms. *Protein Sci.* **28**(11), 1947–1951 (2019).
44. Kanehisa, M., Furumichi, M., Sato, Y., Kawashima, M. & Ishiguro-Watanabe, M. KEGG for taxonomy-based analysis of pathways and genomes. *Nucleic Acids Res.* **51**(D1), D587–D592 (2023).

45. Subramanian, A. *et al.* Gene set enrichment analysis: A knowledge-based approach for interpreting genome-wide expression profiles. *Proc. Natl. Acad. Sci. USA* **102**(43), 15545–15550 (2005).
46. Hänzelmann, S., Castelo, R. & Guinney, J. GSVA: Gene set variation analysis for microarray and RNA-seq data. *BMC Bioinform.* **14**, 7 (2013).
47. Li, T. *et al.* TIMER2.0 for analysis of tumor-infiltrating immune cells. *Nucleic Acids Res.* **48**(W1), W509–W514 (2020).
48. Jani-Acsadi, A., Krajewski, K. & Shy, M. E. Charcot–Marie–Tooth neuropathies: Diagnosis and management. *Semin. Neurol.* **28**(2), 185–194 (2008).
49. Sambuughin, N. *et al.* Autosomal dominant distal spinal muscular atrophy type V (dSMA-V) and Charcot–Marie–Tooth disease type 2D (CMT2D) segregate within a single large kindred and map to a refined region on chromosome 7p15. *J. Neurol. Sci.* **161**(1), 23–28 (1998).
50. Park, M. C. *et al.* Secreted human glycyl-tRNA synthetase implicated in defense against ERK-activated tumorigenesis. *Proc. Natl. Acad. Sci. USA* **109**(11), E640–E647 (2012).
51. Schwarz, R. E. *et al.* Antitumor effects of EMAP II against pancreatic cancer through inhibition of fibronectin-dependent proliferation. *Cancer Biol. Ther.* **9**(8), 632–639 (2010).
52. Awasthi, N., Schwarz, M. A. & Schwarz, R. E. Enhancing cytotoxic agent activity in experimental pancreatic cancer through EMAP II combination therapy. *Cancer Chemother. Pharmacol.* **68**(3), 571–582 (2011).
53. Reznikov, A. G., Chaykovskaya, L. V., Polyakova, L. I. & Kornelyuk, A. I. Antitumor effect of endothelial monocyte-activating polypeptide-II on human prostate adenocarcinoma in mouse xenograft model. *Exp. Oncol.* **29**(4), 267–271 (2007).
54. Bai, X. *et al.* Development and validation of a genomic mutation signature to predict response to PD-1 inhibitors in non-squamous NSCLC: A multicohort study. *J. Immunother. Cancer* **8**(1), e000381 (2020).
55. Guo, L. *et al.* TOX correlates with prognosis, immune infiltration, and T cells exhaustion in lung adenocarcinoma. *Cancer Med.* **9**(18), 6694–6709 (2020).
56. Kidd, P. Th1/Th2 balance: The hypothesis, its limitations, and implications for health and disease. *Altern. Med. Rev.* **8**(3), 223–246 (2003).
57. George, B., Seals, S. & Aban, I. Survival analysis and regression models. *J. Nucl. Cardiol.* **21**(4), 686–694 (2014).
58. Iasonos, A., Schrag, D., Raj, G. V. & Panageas, K. S. How to build and interpret a nomogram for cancer prognosis. *J. Clin. Oncol.* **26**(8), 1364–1370 (2008).
59. Wherry, E. J. T cell exhaustion. *Nat. Immunol.* **12**(6), 492–499 (2011).

Acknowledgements

This research was funded by Natural Science Foundation of Fujian Province (No. 2021J01276, No. 2021J01266, No. 2022J01273) and Quanzhou City Science and Technology Program of China (No. 2023C008YR).

Author contributions

W.L., C.W. and Q.H. organized the article writing and critically modified the manuscript. Z.C. modified the manuscript and drafted the manuscript and was responsible for the acquisition of data. W.Z. check and correct language expression. X.X. and Y.G: Conceptualization, Methodology, Supervision, Writing—review and editing. All authors read and approved the manuscript and agree to be accountable for all aspects of the research in ensuring that the accuracy or integrity of any part of the work are appropriately investigated and resolved.

Competing interests

The authors declare no competing interests.

Additional information

Supplementary Information The online version contains supplementary material available at https://doi.org/10.1038/s41598-024-70041-1.

Correspondence and requests for materials should be addressed to Y.G. or X.X.